PROJECT PAJEX2: FLEXIBLE ADHESIVES

REPORT No 5

FAILURE OF FLEXIBLE ADHESIVE JOINTS

by

Bruce Duncan, Louise Crocker, Jeannie Urquhart,
Elena Arranz, Richard Mera and Bill Broughton

July 2001

NPL Report MATC(A)36

FAILURE OF FLEXIBLE ADHESIVE JOINTS

Project Pajex2: Flexible Adhesives
Report No 5

July 2001

By

Bruce Duncan, Louise Crocker, Jeannie Urquhart, Elena Arranz,
Richard Mera and Bill Broughton

Summary

Flexible adhesives, characterised by low modulus and large extensions to failure, have a long history of use in non-structural applications. However, the advantageous properties of flexible adhesives in sustaining large strains and distributing peel forces more evenly on the bonded substrates is leading to their use for structural joining applications. This is driving the need to improve the understanding of their mechanical properties that have received little attention in comparison to structural adhesives. The study of means of characterising the deformation and failure of flexible adhesives has formed the core of the Flexible Adhesives project of the Performance of Adhesive Joints programme sponsored by the DTI.

The performances of two flexible adhesive types – an elastomer and a polyurethane – have been studied through bulk specimen and adhesive joint tests. Experimental measurements and Finite Element (FE) model predictions, for lap shear, scarf and T-peel joints, have been compared, at different strain rates and temperatures, in an attempt to identify possible failure criteria. No single failure criterion has been identified although a large volume of observations have been made on the behaviour of flexible adhesives. The strength of the adhesive joints correlates well with the tensile strength of the bulk adhesive material measured under corresponding test conditions. Specimens tested at high temperatures and low strain rates have the lowest strength.

Maximum stress values correlate with the tensile strength within a joint configuration but there is no obvious correlation between different joint types. Interpretation is complicated by the dependence of the results on the FE element size. The results suggest that the elastomeric adhesive, where the joints always fail cohesively, can sustain joint stresses that are a higher proportion of the tensile strength than the polyurethane adhesive, where failure modes are more variable. Cracks have been observed to form and grow within the adhesive layer before the maximum load has been reached. Any design or failure criterion will need to relate to the conditions of crack formation rather than ultimate joint strength. Having the predicted maximum principal stress lower than the tensile strength scaled by an adhesive dependant factor of less than one may be a reasonable design criterion.

ISSN 1473-2734

National Physical Laboratory
Teddington, Middlesex, UK, TW11 0LW

Approved on behalf of Managing Director, NPL, by Dr C Lea,
Head of NPL Materials Centre

CONTENTS

1. INTRODUCTION

1.1 BACKGROUND AND OBJECTIVES

Adhesive bonding is increasingly being selected as a joining method for high performance applications and new uses are being made of flexible adhesives in structural roles. Flexible adhesives, characterised by low modulus and large extensions to failure, have a long history of use in non-structural applications, such as footwear bonding, packaging and sealing, where the adhesive is often required to retain joint integrity during large deformations of the adherends. Such applications have rarely required sophisticated predictive design calculations. However, the advantageous properties of flexible adhesives in sustaining large strains and more evenly distributing peel forces on the bonded substrates has led to their use for structural joining applications. Their adoption in industries, such as automotive, where design simulation is used extensively has driven the need to improve the understanding of the mechanical properties of these adhesives. The study of means of characterising the deformation and failure of flexible adhesives has formed the core of the Flexible Adhesives project of the Performance of Adhesive Joints programme sponsored by the DTI.

The flexible adhesive resin material, e.g. a polyurethane, polybutadiene or epoxy-butadiene, will have a glass transition temperature at or below the service temperature and therefore operates in the rubber phase. Tensile modulus values typically range from 1 MPa to 100 MPa and tensile strains at failure are greater than 50 %. Their deformation is characterised by large elastic strains with little evidence of plastic (irrecoverable) deformations. Hence, elastic-plastic material models will be unsuitable for representing these adhesives. Their properties appear similar to rubbers where there is a large body of work on characterising their mechanical behaviour using hyperelastic models [1 – 6]. However, adhesive formulations contain many components not normally present in rubbers and these may cause behaviour not predicted by the models.

There are many hyperelastic models available in Finite Element (FE) modelling packages for characterising rubber materials. However, their suitability for use with flexible adhesives, complex multi-phase materials, has yet to be established. Similarly, combinations of test data under different states of stress are recommended for the determination of model coefficients but some of these tests are not commonly available or particularly suitable for adhesives. The objective of the work presented was to establish suitable models and materials properties data for representing flexible adhesives in design predictions. Knowledge and understanding of the criteria causing failure of the flexible adhesive are a requirement of any safe bond design procedure.

This report discusses the results of an investigation, comparing experimental tests and Finite Element modelling of the performance of three adhesive joint configurations – single lap shear joint (Section 3), scarf or tapered overlap joint (Section 4) and T-peel joint (Section 5). Two flexible adhesives have been used in this work, a single-part elastomeric adhesive and a 2-part polyurethane adhesive, and tests have been performed at various temperatures and strain rates. The objective of the work reported here has been to explore failure criteria for these adhesives although factors affecting accuracy of predictions of deformations are also discussed.

1.2 APPROACHES TO PREDICTING FAILURE

The holy grail of bond strength prediction is to be able to accurately predict the load conditions under which any bonded structure will fail. To succeed in this would require a failure criterion that is valid under any state of stress. In comparison to structural adhesives, there is an extremely limited body of work published on the mechanical performance of flexible adhesives. Even in the field of structural adhesives there is still no generally accepted failure criterion that is valid for all loading states.

There are a number of approaches, listed below, that have been adopted by engineers and designers for predicting the static strength (failure load) of adhesives and adhesively bonded structures that may be relevant to flexible adhesives.

1.2.1 Strength of Materials Based Models [7-15]

Several strength of materials based models (e.g. average stress, maximum stress and maximum strain failure criterion) have been proposed for predicting the strength of bulk adhesives and adhesively bonded joints [7-14];

Average Stress Method: This approach assumes that the strength of the joint is equal to the average shear or normal stress in the adhesive layer at the point of failure (i.e. maximum load). However, the average stress method is unable to account for out-of-plane deformation associated with the eccentricity of the load path and the flexibility of the adhesive and the adherends. The analysis is simplistic, it assumes the adherends are rigid, and that the adhesive only deforms in shear. In fact, the resultant stress distribution, across and along the bond length is very complex and is dependent on adherend and adhesive properties, and joint geometry. Failure results from the combined actions of the peel and shear stress and strain concentrations present at the ends of the adhesive joint.

Maximum Stress Method: This approach, which is widely used in industry, compares the maximum stress in the adhesive layer (normal, shear or von Mises) with the tensile, compressive or shear strength of the adhesive. Failure is deemed to have occurred when the stress exceeds one of the strength values. This approach allows for non-uniform stress distributions along the bond length and through the thickness of the adhesive. Analytical (closed-form equations) or FEA can be used to determine the stress distributions within the adhesive layer. For many applications, closed-form analysis is not feasible for modelling the stress and strain distributions within the adhesive, and hence FEA tends to be used to predict the deformation and strength of bonded structures. A major limitation with FEA is the inability to account for points of stress singularity, such as those present at the ends of bonded joints. The FEA results depend on the element size with the value of the stresses increasing as the element size near the singularity is reduced. If stresses become infinite, then the predicted load at failure is zero. It has been suggested that the element size in regions of high stress gradients be equal to one third of the adhesive thickness [13].

Maximum Strain Criterion: According to Hart-Smith [7-10], maximum lap-joint strength is defined by the adhesive strain energy in shear (i.e. stress level for joint failure is mainly dependent on the shear strain to failure of the adhesive). A maximum strain criterion proposed by Hart-Smith is now widely used within the aerospace industry for determining strength of metallic and composite joints. The analysis developed by Hart-Smith [8, 10] accounts for non-linear elastic-plastic deformation in the adhesive. Arguments can be made that adhesives can sustain very high shear strain and that failure occurs in regions of the joint where tensile

stresses are also present (e.g. the ends of the lap joint). Therefore, the maximum principal strain and dilatational (volumetric) strains may also come into consideration.

Strain Energy Density Criterion: The rupture of pure rubbers is assumed to occur when the strain energy density in the material exceeds the critical energy density of the material, which can be estimated from bulk specimen tests. This approach has been proposed for flexible adhesives [15] and strain energy densities can be output from FE models.

1.2.1 Plastic Yield Criteria and Void Cavitation [16 – 25]

In many materials, the low strain behaviour is characterised by an elastic response and the large strain response by plastic flow behaviour. The transition between elastic and plastic behaviour occurs at the plastic yield point. A number of models have been proposed to predict the onset of plastic yielding under arbitrary stress states.

Tresca Yield Criterion: This criterion was initially developed to describe the yield behaviour of metals and proposes that yield occurs when the maximum shear stress, τ_{max}, reaches a critical value. If $\sigma_1 > \sigma_2 > \sigma_3$ (principal stress components in the 1-, 2- and 3- orthogonal directions) then the criterion is given as [16, 17]:

$$\tau_{max} = \frac{1}{2}(\sigma_1 - \sigma_3) \tag{1}$$

In the case of simple tension:

$$\tau_{max} = \frac{\sigma_1}{2} = \frac{\sigma_y}{2} \tag{2}$$

where σ_y is the yield stress in tension.

The Tresca yield criterion is unable to accurately model the behaviour of polymeric materials under multi-axial loads; as yielding in these materials is sensitive to hydrostatic stress. In response, the Tresca yield criterion has been modified to include the effect of hydrostatic stress. The modified criterion states that the maximum shear stress, τ_{max}, is related to the yield stress in pure shear, τ^o, hydrostatic pressure, p and the pressure sensitivity of the adhesive, μ_t.

$$\tau_{max} = \tau^o + \mu_t p \tag{3}$$

where the hydrostatic pressure, p, is expressed in terms of triaxial stresses σ_x, σ_y and σ_z.

$$p = -\frac{\sigma_x + \sigma_y + \sigma_z}{3} \tag{4}$$

Von Mises Yield Criterion: In this criterion, yield occurs when the shear strain energy in the material reaches a critical value. The critical strain energy value is expressed in terms of the principal stresses by the following symmetric relationship [16, 17]:

$$(\sigma_1 - \sigma_2)^2 + (\sigma_2 - \sigma_3)^2 + (\sigma_3 - \sigma_1)^2 = \text{constant} \tag{5}$$

In the case of simple tension:

$$(\sigma_1 - \sigma_2)^2 + (\sigma_2 - \sigma_3)^2 + (\sigma_3 - \sigma_1)^2 = 2\sigma_y^2 \quad (6)$$

In the case of pure shear, the shear yield stress is predicted to be:

$$\sigma_1 = \sigma_y / \sqrt{3} \quad (7)$$

The von Mises yield criterion, however cannot accurately model the behaviour of rubber-toughened bulk adhesive specimens under tensile, compressive or shear loads; as yielding in these materials is sensitive to hydrostatic as well as shear stress [20]. The von Mises yield criterion has been modified to account for the combined effect of these stresses, and can mathematically be described as follows [19]:

$$\tau_{max} = \tau_m^o + \mu_m p \quad (8)$$

where τ_m denotes the von Mises yield stress, which is defined by the following equation:

$$6\tau_m^2 = (\sigma_1 - \sigma_2)^2 + (\sigma_2 - \sigma_3)^2 + (\sigma_3 - \sigma_1)^2 \quad (9)$$

and τ_m^o is the yield stress in pure shear. The parameter μ_m can be determined from stress/strain measurements under two different stress states.

Alternative yield criterion, such as the Drucker-Prager plasticity model, are available to model polymeric materials but were not investigated in the current work since most of the experimental evidence from bulk specimen tests shows that plastic behaviour is unlikely to be a valid model for the behaviour of flexible adhesives. The von Mises, Tresca and hydrostatic pressure representations of stress described above have been considered in the FE modelling work performed as they provide multi-axial representations of the stress field.

Dean and others at NPL [21] are building on the work of Gurson [22] and Bucknall [23] to develop cavitation models that describe the nucleation and growth of void cavities in structural adhesives and their contribution to plastic deformation of structural adhesives. This work relates to plastic yield phenomena in glassy adhesives and is not directly relevant to flexible adhesives.

1.2.3 Fracture-Mechanics analysis [25-32].

The fracture mechanics approach assumes a pre-existent crack and uses FEA to determine the stress state in the vicinity of the crack tip. It is worth noting that good progress has been made in applying fracture mechanics to predicting crack growth and failure of adhesively bonded joints for single-mode loading configurations [23-32], although the relevance and potential application to actual bonded structures is regarded by the engineering community with some scepticism. Work on fracture energy of adhesive joints has concentrated on structural adhesives with little published on flexible adhesives.

From an engineering perspective, prediction of crack growth rate is considered less important than determining the crack initiation stress or energy. Fracture mechanics test specimens are pre-cracked, a situation the adhesive bonder will strive to avoid in bonded structures. To apply

fracture mechanics to un-cracked specimens an initial defect or flaw must be assumed to be present in regions of high stress gradients (e.g. adhesive fillets). Estimating the size and shape of this flaw introduces uncertainties into the analyses. For these reasons the fracture mechanics approach has not been considered in this work, which has concentrated on a continuum mechanics approach.

It has been suggested that failure occurs when the maximum stress/strain exceeds a critical stress/strain value at a distance, or when the stress acting over a certain volume exceeds a critical value [32]. The critical distance or volume, which is generally defined using FEA and experimental data, is a function of the specimen geometry and size, and the defect spectrum contained within the specimen. The adhesive in regions of high-localised stresses (e.g. joint fillets) may be intrinsically stronger than bulk adhesive test specimens because the former is less likely to contain a critical flaw. Weibull statistical analysis can be used to model the sensitivity of both distance and volume failure criteria to changes in local geometry and singularity strength (see [32]).

2. EXPERIMENTAL

Since flexible adhesives are visco-elastic materials, care needs to be taken to ensure that the tests performed under different states of stress are carried out under similar test temperatures and rates of strain in the adhesive layer. All tests were carried out in environmental chambers with the temperatures controlled to ± 0.3 °C or better. The control of strain rates in each test is discussed below.

2.1 ADHESIVES

Two flexible adhesives, a single-part elastomer M70 supplied by Evode Ltd and a two-part polyurethane DP609 supplied by 3M Ltd were used in this study. These adhesives were mainly characterised using tensile test methods and details of these have been reported elsewhere [33, 34]. Tensile tests were performed in an Instron 4505 test machine fitted with low capacity load cells (100 N and 1000 N load cells were used) to measure force (F). Test specimens were clamped with the grips positioned to maintain a free specimen length of 63 ± 3 mm to minimise uncertainties in the strain rates. All tests were carried out at one of the test speeds chosen for the work (1, 10 or 100 mm min^{-1}). Strains were determined, from contrasting gauge marks on the specimen surface, using a Messphysik video extensometer. This instrument simultaneously measures axial extensions (ΔL) and contraction of the specimen width (Δw). These measurements are used to obtain stress (σ) axial strain (ε_a) and lateral strain (ε_l) values:

$$\textit{axial strain} \quad \varepsilon_a = \frac{\Delta L}{L_0} = \frac{L - L_0}{L} \quad \textit{and} \quad \textit{true strain}, \quad \varepsilon_T = \ln(1 + \varepsilon_a) \tag{10}$$

$$\textit{lateral strain} \quad \varepsilon_l = -\frac{\Delta w}{w_0} = \frac{w_0 - w}{w_0} \tag{11}$$

$$\textit{stress} \quad \sigma = \frac{F}{w_0 t_0} \quad \textit{and} \quad \textit{true stress} \quad \sigma_T = \frac{F}{wt} = \frac{F}{w_0 t_0 (1 - \varepsilon_l)^2} = \frac{\sigma}{(1 - \varepsilon_l)^2} \tag{12}$$

where L_0, w_0 and t_0 are the initial gauge length, width and thickness respectively. L, w and t are the values of these dimensions at any point during the test. The assumption is made that lateral strains are constant in the width and thickness directions (i.e. $\Delta w/w_0 = \Delta t/t_0$).

Volumetric strain ratios (ε_v) can be calculated from the measured axial and lateral strains [35]:

$$\varepsilon_V = \frac{V}{V_0} = (1+\varepsilon_a)(1-\varepsilon_l)^2 \quad (13)$$

2.1.1 Elastomer M70

The Evode M70 elastomer is a single-part, heat-curing adhesive, supplied in 300 ml cartridges. It is coloured black. The paste has a high viscosity and does not flow easily. To manufacture thin sheets of this adhesive it was necessary to spread layers of the adhesive onto release film coated metal plates using a spatula [36, 37]. Thin polymer strips were used as spacers and the moulds were closed with a second release film coated metal plate.

The sheets were placed in a pre-heated oven and cured in the mould at 200 °C for 45 minutes. Glass transition temperatures (T_g), measured using dynamic mechanical thermal analysis (DMTA), averaged -33 ± 2 °C. This cure state was the 'standard' cure state for the samples used in this study. Cure schedules were devised for the various joint specimens that approximated the thermal history measured during cure of the bulk material.

The hand spreading of the adhesive is a method that can introduce air bubble voids into the specimens. These are difficult to detect in the sheets manufactured due to the black colour of the adhesive. However, voids can be seen on the edges of cut test specimens and on the fracture surfaces after tests indicating their presence throughout the samples. These voids will act as stress concentrators, limiting the ultimate strength available from bulk specimens. Thus, the bulk specimen tests ought to provide a conservative estimate of the strength of the material in joints.

The mechanical properties of the M70 elastomer were characterised using uniaxial tension, planar tension and equi-biaxial tension tests [38, 39]. Volumetric properties were obtained from uniaxial tension measurements with simultaneous measurement of axial strain and lateral contraction [35]. Previous findings indicated that the uniaxial tension data were sufficient to characterise the mechanical properties of the adhesive and that adding the planar and biaxial test data had limited effect on the accuracy of predictions [40].

Test data obtained from uniaxial tension tests at various temperatures and strain rates [33] are summarised in Table 1. Modulus, strength and strain to failure all decrease with increasing temperature. Plots of true-stress against true-strain were virtually linear, indicating an absence of plastic behaviour. The slopes of these lines were calculated by linear regression to estimate modulus. Local strain energies at failure were estimated from the areas under the true-stress against true-strain curves.

Temp	Strain Rate	Axial strain at failure	Stress at failure	Young's modulus	Poisson's ratio	lateral strain at failure	true strain at failure	true stress at failure	Strain Energy
°C	s^{-1}		(MPa)	(MPa)				(MPa)	J mm^{-3}
0	3 x 10^{-4}	0.422 ± 0.07	3.12 ± 0.22	11.3	0.27	0.114	0.352	3.974	0.70
0	3 x 10^{-3}	0.468 ± 0.08	3.87 ± 0.24	13.1	0.26	0.122	0.384	5.017	0.96
0	3 x 10^{-2}	0.491 ± 0.12	5.51 ± 1.57	17.9	0.25	0.123	0.399	7.160	1.43
0	8 x 10^{-2}	0.340 ± 0.14	5.01 ± 0.88	20.9	0.28	0.095	0.293	6.120	0.90
20	3 x 10^{-4}	0.390 ± 0.10	2.19 ± 0.57	8.5	0.30	0.117	0.329	2.809	0.46
20	3 x 10^{-3}	0.487 ± 0.05	2.87 ± 0.28	9.8	0.29	0.141	0.397	3.892	0.77
20	3 x 10^{-2}	0.484 ± 0.09	3.50 ± 0.35	11.6	0.26	0.126	0.395	4.580	0.90
20	8 x 10^{-2}	0.420 ± 0.07	3.79 ± 0.43	13.6	0.26	0.109	0.351	4.776	0.84
40	3 x 10^{-4}	0.289 ± 0.05	1.92 ± 0.26	9.1	0.30	0.087	0.254	2.302	0.29
40	3 x 10^{-3}	0.344 ± 0.06	2.26 ± 0.21	9.6	0.31	0.107	0.296	2.832	0.42
40	3 x 10^{-2}	0.403 ± 0.09	2.77 ± 0.25	10.4	0.28	0.113	0.339	3.519	0.60
40	8 x 10^{-2}	0.353 ± 0.04	2.87 ± 0.17	11.8	0.29	0.102	0.302	3.562	0.54
80	3 x 10^{-4}	0.221 ± 0.04	1.46 ± 0.34	8.6	0.35	0.077	0.200	1.715	0.17
80	3 x 10^{-3}	0.268 ± 0.03	2.05 ± 0.09	10.5	0.35	0.094	0.237	2.496	0.30
80	3 x 10^{-2}	0.237 ± 0.06	2.11 ± 0.27	11.8	0.35	0.083	0.213	2.509	0.27
80	8 x 10^{-2}	0.310 ± 0.06	2.39 ± 0.46	11.1	0.35	0.109	0.270	3.007	0.41

Table 1: Tensile properties of the single-part elastomer adhesive

2.1.2 Polyurethane DP609

The polyurethane (PU) adhesive DP609 was supplied by 3M Ltd in 400 ml twin pack cartridges. These are dispensed, using a pneumatic gun, through static mixing nozzles that ensure thorough mixing of the adhesive. Due to the visco-elastic properties of the two adhesive components, flow can continue into the mixing nozzle after the pressure is released and, thus, cause regions of incorrectly mixed material that are significantly weaker than the correctly mixed materials. To avoid this, each sample was cast in a single action with dispensing pressure maintained continuously. The two components should mix to a uniform brown colour. Any streaks in the sample indicate non-uniform mixing. In thin sheets the material is sufficiently transparent to allow visual detection of voids.

Adhesive sheets were cast using either 0.5 mm or 1.0 mm spacers to control thickness. The PU sheets were allowed to cure overnight before being released from the mould. All samples were left to cure for 7 days before being post-cured for 90 minutes at 50 °C. The post-cure was carried out to minimise any further changes in cure state during the period when samples were tested. Glass transition temperature measurements T_g, by the dynamic mechanical thermal analysis method stayed constant, around 17 °C, over a 3 month period following post-cure.

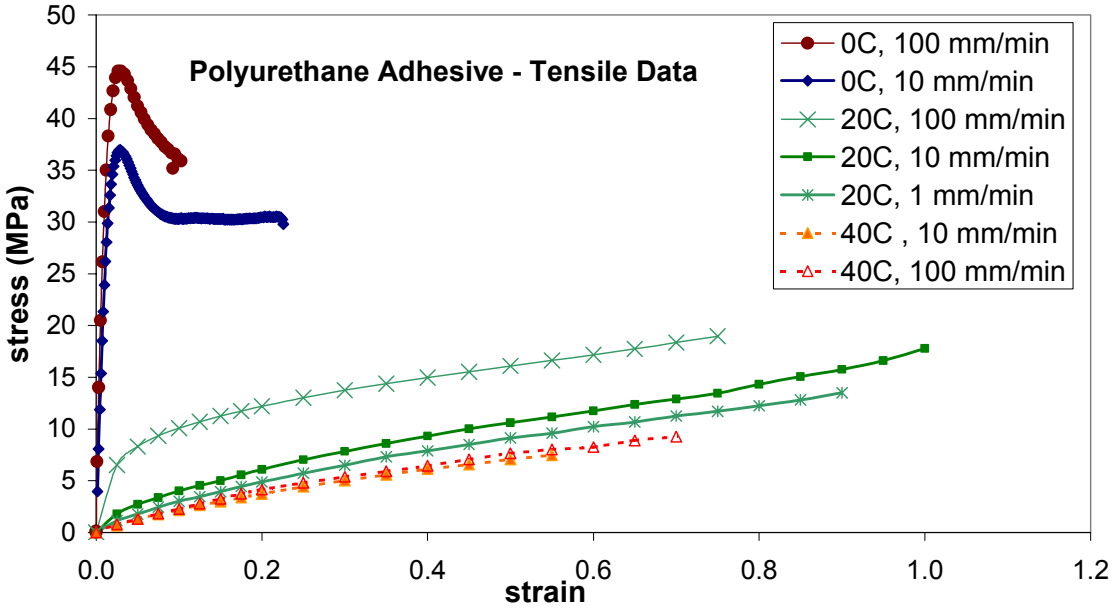

Figure 1: Tensile properties of polyurethane adhesive

The mechanical properties, characterised using uniaxial tension tests [34] are summarised in Table 2 and Figure 1. At 0 °C the material is glassy and the stress-strain curve contains a peak at low strains, which is consistent with plastic yield behaviour. Elastic-plastic models can be used to characterise the behaviour of this adhesive at low temperatures. Since this report concerns flexible adhesives further discussion of the properties of the PU adhesive at low temperatures is omitted. Although the maximum stress is high, the strain to failure and, hence, energy absorbing properties are low. The energy absorption is highest at 20 °C, close to T_g, although the stain rate dependence is high. The strains to failure and failure strengths are significantly lower at the higher temperature 40 °C.

T	Speed	Rate	max stress	max strain	true stress	true strain	volume ratio	E	Poisson's ratio	Energy
°C	mm min^{-1}	s^{-1}	MPa		MPa			MPa		J mm^{-3}
0	100	2.96 x 10^{-2}	44.78 ±0.84	0.029 ±0.002	45.6	0.029	1.01	3110	0.288	0.66
0	10	3.00 x 10^{-3}	38.17 ±1.45	0.027 ±0.003	38.8	0.026	1.01	2200	0.332	0.51
20	100	2.96 x 10^{-2}	21.56 ±1.94	0.901 ±0.13	33.8	0.640	1.21	52	0.233	10.82
20	10	3.03 x 10^{-3}	15.78 ±2.35	0.864 ±0.16	23.8	0.619	1.24	30	0.231	7.37
20	1	2.90 x 10^{-4}	13.72 ±0.91	0.904 ±0.04	21.0	0.644	1.25	31	0.239	6.75
40	100	3.01 x 10^{-2}	8.79 ±0.95	0.625 ±0.10	12.3	0.484	1.16	25	0.242	2.98
40	10	3.00 x 10^{-3}	7.08 ±1.13	0.563 ±0.06	9.6	0.446	1.15	19	0.273	2.14

Table 2: Tensile properties of PU adhesive

2.2 ADHESIVE JOINT TESTS

The experimental details of each of the three adhesive joint tests are discussed in later sections. The approaches taken for preparing the test specimens were similar for each joint. All adherends were fabricated from mild steel. The adherends in the lap joint and the scarf tests were considered to be almost infinitely rigid in comparison to the low modulus adhesives and it was thought unlikely that any stresses would exceed the yield stress of over 200 MPa.

All adherends were pre-treated through an acetone wipe to degrease the specimen followed by grit blasting using an aluminium oxide abrasive to roughen the surface and remove weakly adhering layers. All adherends were then acetone wiped prior to either bonding or priming.

The elastomeric adhesive could be bonded directly to the prepared steel surfaces. All of the test specimens failed cohesively in the adhesive layer. The steel surfaces required priming to improve the bond to the polyurethane adhesive. The epoxy-based primer 3M 1945 B/A was obtained from 3M Ltd. Adherends were primed following manufacturers instructions. The two parts were vigorously agitated in order to fully disperse the components. These were then mixed in equal volumes and allowed to react for a further hour (with periodic stirring) before the mixed system was painted onto the adherends to form a single, continuous coat. The primed adherends were left to dry overnight. Specimens were acetone wiped as a further degreasing stage prior to bonding.

2.3 FINITE ELEMENT ANALYSIS

The details of the FE models run for each joint test – single lap shear, scarf joint and T-peel – are discussed in later sections. However, there were common approaches taken for all specimens.

In any FE model there is a trade off between model complexity and resources (time and computational) required to produce results. The model needs to be sufficiently detailed to realistically represent the component, particularly in regions of critical importance, while minimising the complexity of the mesh to optimise run times. Since for bonded structures the performance of the adhesive bond is critical to the joint strength, element density is normally higher in the bond line than in the adherends. This is normally further refined by increasing element density towards the end of the bond line (where stress concentrations are normally expected) at the expense of the centre of the bond (where stress will be more uniform). The effects of meshing are discussed in later sections.

2.3.1 Software

All FE models were run using the ABAQUS/STANDARD version 5.8 solver supplied by HKS Ltd [41]. In general, the *STATIC – time-independent - analysis routines were used. However, where visco-elastic properties were modelled the *VISCO – time-dependent – analysis routines were used. All FE meshes were produced using the FEMGV pre-processor software supplied by FEMSYS Ltd [42].

2.3.2 Constraints and Adherends

At one end of the specimen, nodes were constrained from movement in the 1, 2 and 3 directions (corresponding to x, y and z axes where x is the direction in which the specimen is loaded) in order to simulate a fixed grip. At the other end of the specimen all nodes were tied to a reference node. These were constrained in the 2 and 3 directions whilst a displacement was applied in the 1 direction to simulate extension in the test machine. The total reaction force on the specimen is summed at the end node. This arrangement does not fully model the test machine – no allowance is made for the compliance of the test machine (particularly the out of plane compliance) or any imperfections in the test machine set-up (e.g. misalignment).

The metal adherends were modelled as elastic-plastic materials. The mild steel used for the adherends was assumed to have a tensile modulus of 213.6 GPa and a Poisson's ratio of 0.296. The plastic yield stress of the steel was assumed to be over 200 MPa. The thick adherends in the scarf joint test are unlikely to be loaded sufficiently to lead to plastic yielding of the adherends. However, the thin, 1.5 mm gauge steel used to make the lap shear and the T-peel test specimens will experience higher stress levels and plastic deformation of the adherends is possible. If an estimate of 200 MPa is made for the yield strength then plastic deformation of the adherends is a possibility at forces around 600 N in the T-peel test and 1800 N in the lap joint test. Both these loads are greater than achieved in the joints bonded with the elastomer adhesive but not for those bonded with the PU adhesive.

2.3.3 Models for the Adhesive Layer

The adhesive layer was modelled as a hyperelastic material. Hyperelastic models [1-6, 40 41, 43], such as the polynomial model, have similar formulations and derive energy potentials (U) from a combination of first and second order deviatoric strain invariants I_1 and I_2 (with fitted coefficients C_{ij}) and elastic volume matrix J^{el} (with fitted coefficients D_i).

$$U=\sum_{i+j=1}^{N} C_{ij}\left(I_1-3\right)^{i}\left(I_2-3\right)^{j}+\sum_{i=1}^{N}\frac{1}{D_i}\left(J^{el}-1\right)^{2i} \qquad (14)$$

The higher the model order (N) the more complex the function and the greater the number of constants. Higher order functions are required to fit the complex shapes of the stress-strain curves of true high-strain rubbers but may lead to instability in the FE solver code causing convergence problems in analyses. Since most flexible adhesives do not sustain strains greater than ca. 1.0, the lowest order models (N=1) should be most appropriate. For polynomial models, the N=1 case is the classical Mooney-Rivlin model [1]. Other first order models are the Neo Hooke (reduced polynomial with N=1) and Arruda-Boyce [2]. Polynomial, reduced polynomial and Ogden [3] models are available in FEA packages with orders N = 1, 2 or 3.

The influences of material models and the types of input data have been discussed in a previous report [40]. The results of some analyses performed with a variety of material models and input data are briefly discussed in this report but it is not the intention of this report to repeat these previous discussions. Most of the FE analyses described in this report were performed using the Mooney-Rivlin model with input data (including volumetric terms) derived from uniaxial tension data. The Mooney-Rivlin model was selected as, while it may not have been the most accurate of the models investigated earlier, it is widely implemented in FE software packages. When hyperelastic models of order 2 or higher were used to represent

adhesives in FE simulations of bonded joint specimens it was often noticed that the shapes of the predicted curves did not match those of the first order models or measured test data.

In the analyses discussed in this report, based on earlier findings, the input data were derived from uniaxial tensile tests unless otherwise noted. Uniaxial tension, referred to as tensile, data were supplied as sets of pairs of (engineering stress, engineering strain) points. Volumetric data were supplied as sets of pairs of (–1 x true stress, volume ratio) points [35].

2.3.4 Stress Analysis

One of the major uses of Finite Element modelling is to map the stress distributions in components and structures in order to identify and quantify regions of high stress. These stress concentrations are critical to the performance of the structure. Failure, whether through a monotonic increase in stress beyond the rupture strength of the material or accumulation of fatigue damage, will tend to initiate in these regions. If accurate failure criteria are known then these regions can be assessed to determine if, under service loading, they will compromise structural performance.

In the results discussed in later sections, the stress and strain predictions were taken from contour plots of the components rather than averaged within an element. This will tend to produce slightly higher maximum values although both techniques will produce results that are sensitive to any numerical singularities in the structure. It has been previously noted that the FE model predictions tend to be stiffer than the measured joint responses. Thus, the models do not produce any increments where both load and extension approximate those determined at the peak load in the tests. Since maximum loads seemed more reproducible in the tests than the maximum strains (whose accuracy is limited by the accuracy to which a thin bond line can be measured), the predictions were normally made at fixed loads (generally the average load at failure for the joint type under a set of test conditions). This means that the strain predicted in the joints could be significantly lower than those actually occurring in the adhesive layer. For this reason, investigations have concentrated on relating stress components to material strength.

The stress and strain components extracted from the ABAQUS FE models are described in Appendix I. All of the stress and strain components are calculated as ‘true’ values rather than apparent or engineering values.

3. LAP SHEAR JOINTS

The single lap shear joint test [44-46] is ubiquitous in the assessment of adhesives and bonded systems by industry. Although bending of the adherends and rotation of the bond line introduce non-uniform stress states in the adhesive preventing the accurate determination of material properties this test is often used as the primary screening test for adhesives and surface preparations.

The single lap shear joint is often considered as a '2 dimensional' system with strength scaling directly with the adherend width w. Results are often expressed as loads per unit width P in order to compare different tests. For any value of P stress and strain levels should be independent of w provided that the other specimen dimensions remain constant. All the lap joint adherends used in the work discussed in this report were 25 mm wide removing any requirement to normalise by w in order to compare results. However, the overlap length l was variable and results were normalised by overlap length to aid comparisons.

Analytical formulations [47] have been derived for the average shear stress σ_s and normal stress σ_{an} in terms of P, overlap length l and bond line thickness t:

$$\sigma_S = \frac{P}{l} \qquad \text{and} \qquad \sigma_{an} = \frac{3P}{(l+t)} \tag{15}$$

Equation (15) indicates that the average normal stress decreases with increasing bond thickness. This ought to translate to an increase in bond strength with bond thickness although this is misleading as increasing bond thickness leads to more bond rotation and, hence, higher peel stresses at the end of the bond line.

3.1 LAP SHEAR EXPERIMENTS

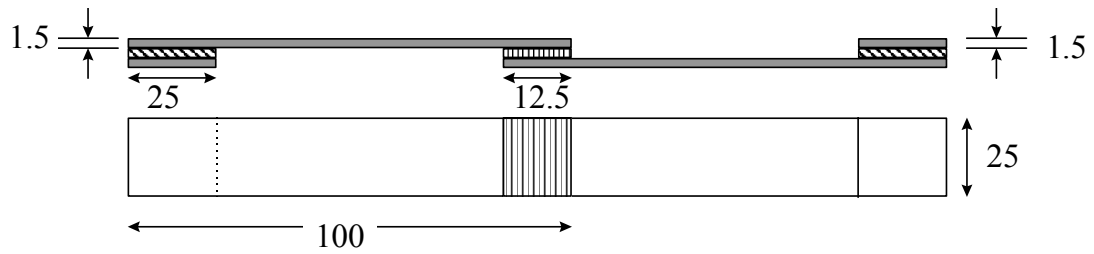

Figure 2: Lap Joint Test Specimen (dimensions in mm)

The standard single lap shear joint specimen used in this work is shown in Figure 2. Tabs, cut from the same material, were bonded at each end to improve alignment and reduce the eccentricity of the load path that causes out-of-plane bending when the specimen is tested. The mild steel adherends were 100 mm long by 25 mm wide by 1.5 mm thick. Specimens were bonded in a jig to ensure alignment and control the overlap length. The standard overlap length used was nominally 12.5 mm although some tests were performed with larger overlaps (25 mm and 50 mm). Specimens were bonded with bond lines between 0.25 mm and 1.0 mm thick. The thickness of the bond line was controlled by either mixing glass beads into the adhesive or inserting wires into the bond lines.

The size and shape of the fillet at the end of the bond line in the lap joint specimen determines the stress concentration that will eventually lead to failure. No attempts were made to control

the size or shape of the spew fillet during manufacture. Instead these were cut off after cure to form a square end. This shape of fillet increases the stress concentration at the end of the joint and is probably a 'worst case' scenario for the lap joint. It is recognised that removal of the fillet could lead to damage to the end of the adhesive layer; thereby leading to premature failure. Consideration was given to radiussing the adhesive fillets to reduce stress concentrations but this was rejected owing to the difficulties of producing exact, reproducible fillet shapes and the large effort required. A number of specimens were prepared with large excess fillets that were not removed. Provided that the fillet is large enough, the ends of the fillet carry little load and the joint performance ought to be independent of the shape of the end of the fillet.

The lap joints were tested using an Instron 4507 test machine fitted with an Instron temperature chamber. The shear extension was measured using a pair of 25 mm gauge length Instron type 2602 extensometers attached straddling the bond line. Specimens were tested at the same temperatures as the tensile specimens (0, 20, 40 °C). Test speeds were selected, depending on the thickness of the adhesive layer, in order to obtain shear strain rates in the bond line that were approximately the same as the strain rates in tensile tests. The results obtained [33, 34] are shown in Tables 4 and 5.

Temp	**strain rate**	**load**	**load/length**	**strain (ext/thick)**
(°C)	(1/s)	(N)	(N/mm)	(mm/mm)
0	$3x10^{-4}$	791 ± 100	64.5 ± 6.7	1.18 ± 0.24
0	$3x10^{-3}$	864 ± 80	73.6 ± 6.1	1.44 ± 0.32
0	$3x10^{-2}$	1094 ± 55	90.4 ± 5.3	1.50 ± 0.20
20	$3x10^{-4}$	535 ± 55	44.8 ± 4.0	1.01 ± 0.08
20	$3x10^{-3}$	612 ± 13	51.0 ± 3.8	1.08 ± 0.23
20	$3x10^{-2}$	729 ± 46	59.8 ± 4.9	1.11 ± 0.37
40	$3x10^{-4}$	413 ± 56	32.9 ± 4.7	0.90 ± 0.23
40	$3x10^{-3}$	496 ± 90	39.9 ± 7.8	1.12 ± 0.16
40	$3x10^{-2}$	543 ± 50	45.0 ± 4.4	1.22 ± 0.33

Table 4: Lap joint failure results – elastomeric adhesive [33]

Temp	**Strain rate**	**Load**	**Bond thickness**	**Strain**	**load/length**
(°C)	(1/s)	(N)	(mm)		(N/mm)
40	$4.\ 2x10^{-3}$	1227 ± 315	0.21 ± 0.05	0.65 ± 0.44	95.5 ± 26.3
20	$3.\ 2x10^{-3}$	2051 ± 481	0.22 ± 0.02	0.71 ± 0.37	160.9 ±40.1
20	$3.\ 3x10^{-3}$	2430 ± 649	0.22 ± 0.17	1.18 ± 0.49	185.9 ± 48.9
20	$2.4x10^{-2}$	2867 ± 1156	0.21 ± 0.03	0.81 ± 0.37	222.0 ± 79.6
0	$3x10^{-3}$	2962 ± 354	1.04 ± 0.04	0.085 ± 0.07	209.1 ± 29.5

Table 5: Lap joint failure results – PU adhesive [34]

3.2 LAP JOINT FINITE ELEMENT ANALYSIS

Since the lap shear joint can be considered a 2-dimensional problem most of the FE analyses were performed using 2-dimensional models. Some 3-dimensional analyses were performed and showed that the stress is essentially independent of the width of the specimen. Lap shear joint specimens were meshed to correspond to the geometries tested. In all cases the adherends were mild steel, 100 mm long by 25 mm wide. Models were created with overlap lengths of 12.5, 25 and 50 mm and bond line thickness 0.25, 0.5 and 1.0 mm. Various element types and densities were explored in the FE studies. Some fillet geometries were also explored. Typically, models were run with constraints applied only to the ends of the adherends as shown in Figure 3. Since the adherends are considerably stiffer than the bond line, there were no significant differences from the results of analyses using models where the whole of the tabbed ends were constrained. This would not necessarily be the case with more rigid, structural adhesives.

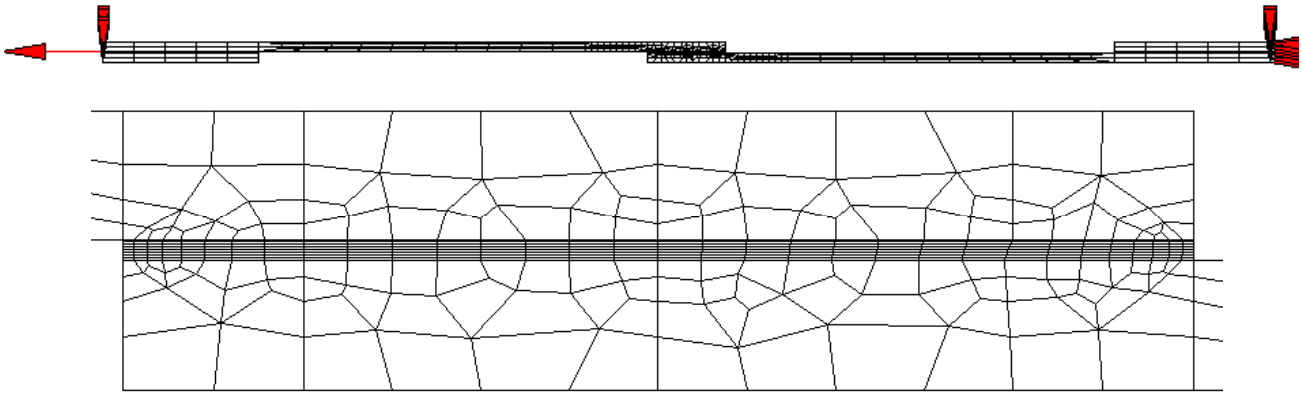

Figure 3: Typical mesh for lap joint specimen

Analyses of stress levels in the adherends of lap joints bonded with the PU adhesive indicated that, in very small regions, the yield stress of the steel might be exceeded during the tests. Further FE analyses were run with a reduced yield stress of the steel to assess the influence of the plastic properties of the adherends. The results were essentially the same as the original analyses indicating that any yielding of the steel would be very localised and have insignificant effect on the joint performance. Test specimens showed no obvious signs of bending after testing.

Results of stress analyses on the elastomeric adhesive specimens are shown for the standard lap joint (overlap length 12.5 mm, bond thickness 0.25 mm and no fillet) modelled using the Mooney-Rivlin model and second-order plane strain elements, with reduced integration and hourglass stiffening (CPE8RH), in Table 6. The strain column represents the predicted joint extension divided by bond layer thickness (0.25 mm) at the normalised failure load. The results for the PU adhesive (modelled using a different mesh and CPE4 elements) are shown in Table 7. In both Table 6 and Table 7 the analyses results were obtained at the failure loads quoted. The maximum values of the stress and strain components scale with the loads at failure.

Temp	Strain Rate	Load/overlap	Strain	E12	EP3	S11	S22	S12	SP3	MISES	SENER
°C	s^{-1}	N/mm				MPa	MPa	MPa	MPa	MPa	J/mm^3
40	$3x10^{-4}$	32.9	0.40	-0.59	0.38	2.86	2.97	-1.89	4.75	3.29	0.59
40	$3x10^{-3}$	39.9	0.46	-0.71	0.43	3.83	3.58	-2.44	6.03	4.25	0.86
40	$3x10^{-2}$	45.0	0.45	-0.69	0.42	4.04	4.03	-2.64	6.57	4.59	0.92
20	$3x10^{-4}$	44.8	0.49	-0.77	0.48	4.34	3.95	-2.73	6.75	4.78	1.06
20	$3x10^{-3}$	51.0	0.53	-0.82	0.51	5.08	4.47	-3.16	7.78	5.55	1.28
20	$3x10^{-2}$	59.8	0.48	-0.72	0.46	5.27	5.26	-3.47	8.58	6.03	1.33
0	$3x10^{-4}$	64.5	0.63	-0.96	0.60	6.44	5.33	-3.97	9.66	7.03	1.94
0	$3x10^{-3}$	73.6	0.55	-0.83	0.53	6.72	6.27	-4.32	10.59	7.56	1.92
0	$3x10^{-2}$	90.4	0.46	-0.67	0.44	7.53	8.09	-5.10	12.67	8.91	1.93

Table 6: Maximum stress and strain components predicted in elastomer lap joints

Temp	Strain Rate	Load/overlap	Strain	E12	EP3	S11	S22	S12	SP3	MISES	SENER
°C	s^{-1}	N/mm				MPa	MPa	MPa	MPa	MPa	J/mm^3
40	$3x10^{-3}$	95.5	0.50	-0.61	0.34	5.44	5.52	-5.11	10.59	8.91	1.82
20	$3x10^{-4}$	161	0.68	-0.78	0.45	10.52	8.72	-8.66	18.37	15.27	4.06
20	$3x10^{-3}$	186	0.63	-0.73	0.42	11.25	10.40	-9.96	20.81	17.43	4.30
20	$3x10^{-2}$	222	0.36	-0.39	0.24	9.82	14.56	-11.96	24.18	21.58	3.22

Table 7: Maximum stress and strain components predicted in PU lap joints

It is recognised that various modelling factors may affect the results of the FEA modelling. The most significant of these – element type, element size, input data source are discussed in sections 3.2.1 to 3.2.3 below.

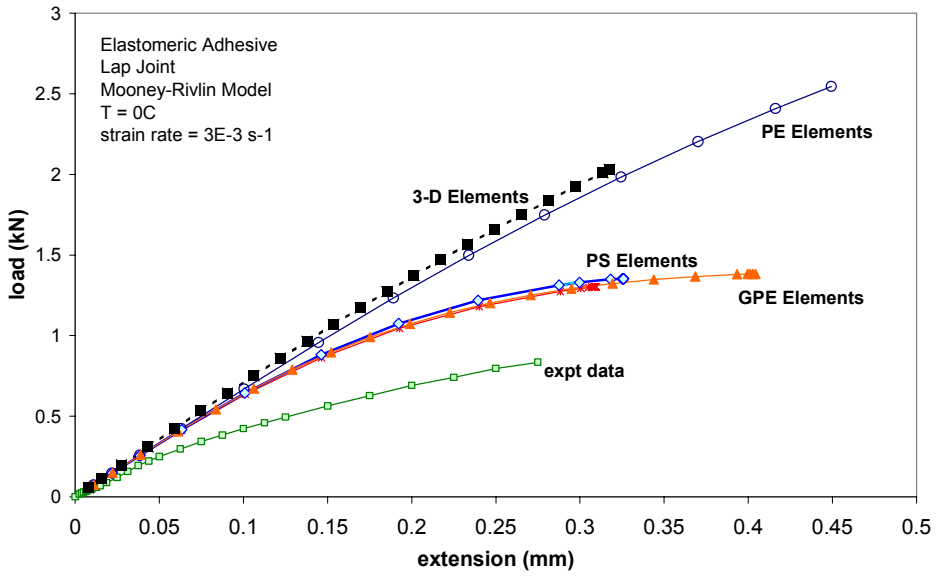

Figure 4: Comparison of different element types

3.2.1 EFFECT OF ELEMENT TYPE

It is known that the general type of element used in FEA can affect the predicted force-extension curve. The effects of these element types on maximum stress and component values were also investigated.

Comparisons made between the general types of element - 2-dimensional plane strain (PE), 2-dimensional plane stress (PS), 2-dimensional generalised plane strain (GPE) and 3-dimensional cubic - are shown in Figure 4. PE elements are recommended for 2-dimensional structures where materials are highly constrained in the out-of-plane direction, e.g. an adhesive bonded between two rigid adherends. GPE elements allow some strain in the out-of-plane direction and allow some inclusion of Poisson's contraction effects. This is achieved by tying all elements to two 'dummy' nodes. The alternative element type, plane stress PS, allows for out-of-plane strains and is suitable for unconstrained materials (e.g. a free plate). This element type was not considered suitable for adhesives in bonded joints.

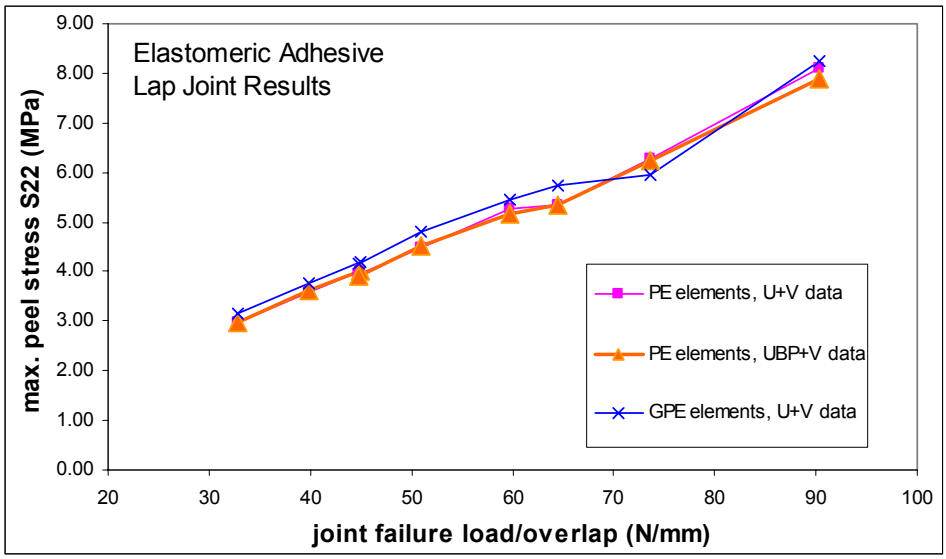

Figure 5: Effect of element and input data type on predicted stress concentrations

The lap joint was modelled using input data for the elastomer adhesive obtained from uniaxial tension tests at a strain rate of $3x10^{-3}$ s^{-1} and a temperature of 0 °C. The material model used was the Mooney-Rivlin model. As Figure 4 shows the plane strain analysis appears to give a better approximation of the 3-D analysis than the generalised plane strain analysis. However, none of the models accurately predicts the experimental data although the generalised plane strain elements are closest. If the adhesive is modelled using PS elements then the results are similar to those obtained using GPE elements. The results were independent of the type of element used to model the steel adherends – the prediction is dominated by the behaviour of the adhesive layer. Varying the exact type of element used (e.g. first or second order element, standard or reduced integration, hour glass stiffening) did not lead to any significant deviations from the predicted responses of the general element type.

Comparing stress analyses, performed using the same FE mesh density, at corresponding loads (Figure 5) showed that the type of element selected has little influence on the maximum stress values predicted in 2-dimensional analyses. Where 2- and 3-dimensional analyses have been compared there have not been any significant differences between predicted maximum stress and strain values. There appeared to be differences between the stress distributions predicted

for first-order elements (e.g. CPE4) and second-order-elements (e.g. CPE8) but these are considered to be due to the effective element area and are discussed in the section on the effects of element size.

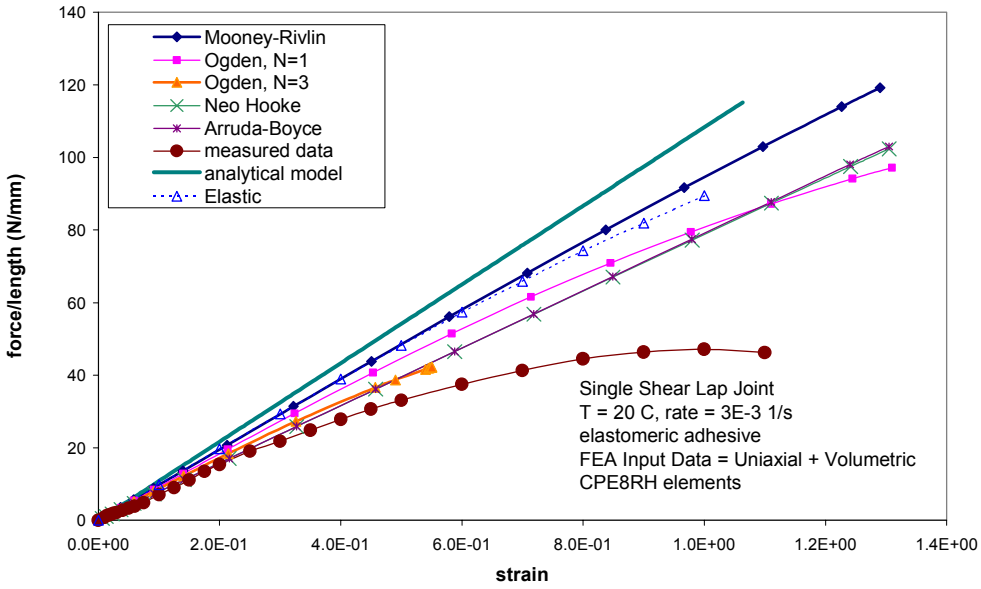

Figure 6: Effect of material model on force-extension predictions

3.2.2 Effect of Material Model and Input Data

Earlier work [40] showed that the choice of material model and input data effects the force-extension predictions (Figure 6). However, when values of peak stress concentrations, such as peel stress shown in Figure 7, are predicted at loads equal to the average of the experimentally determined failure loads the differences between the models are minimal. There appears to be a direct correlation between the measured failure load and the corresponding predicted maximum stress value. The type of input data selected does not appear to have any significant effect on the maximum stress values predicted under any given load (Figure 7).

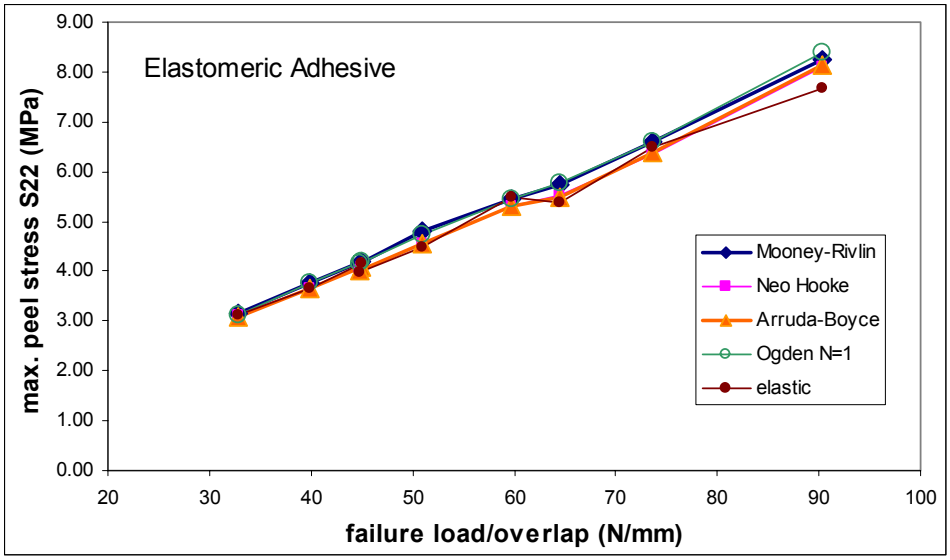

Figure 7: Effect of material model on predicted stress

3.2.3 Effect of Element Size

In theory, more refined meshes ought to give a better representation of the component being modelled. However, larger numbers of elements make the problem larger and, hence, require more computational resource to solve. The larger the number of elements the longer the analysis will take to run. In an adhesive joint the critical region for failure is usually near the ends of the bond line. Therefore, this region is usually modelled with a larger number of elements than other less critical regions of the component (such as the centre of the bond line or the adherends).

Altering the mesh density and, hence, the average size of each element has little effect on the predicted force-extension curves. However, the predicted stress concentration at the end of the bond line does depend significantly on the size of the elements in the mesh. The FEA predicts a stress singularity at the ends of the joint since the lap joint was modelled without a fillet and the adherend ends were assumed to be square. The element at the corner has an extremely high stress gradient. Reducing the element size seems to further concentrate the stress and gives an apparent higher peak stress value for the same load, as shown in Figure 8. Second-order elements (elements with mid-side nodes) appear to predict higher stress concentrations than similar sized first-order elements. However, the additional nodes in the second-order elements can be thought of as increasing the resolution of stress predictions within the element, effectively acting as a smaller-area element. Reducing the area of the element by a factor of 4 to account for this brings a better agreement between first and second-order element predictions.

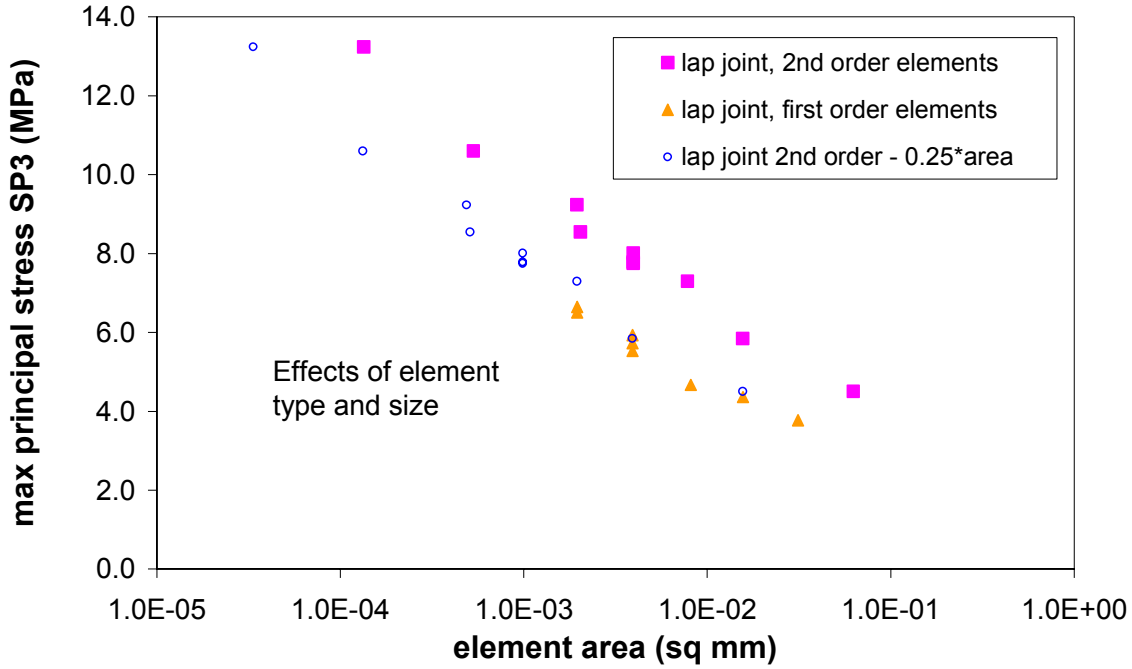

Figure 8: Effect of element size on FEA predicted stress concentration (elastomer)

This significant dependence of predicted stress concentration values on element size causes much difficulty in attempting to interpret failure criteria from the results. Any comparisons between different joint geometries are immensely complicated by the dependence of the results on element size.

3.3 FILLET SHAPES

3.3.1 Comparison of No Fillet and Long Fillet Specimens

The critical stresses at the end of the bond line in a lap shear joint depend on the precise geometry of the adherends and glue line in this region. These are difficult to control in practice. Specimen preparation with shaped adherend ends and fillets are expensive to produce and impractical if large quantities of test specimens are to be prepared.

The ends of the adherends were not modified beyond any effects of the surface preparation (grit blasting). These were assumed to be square. However, examination of the ends of the adherends determined that not all of the steel strips had been guillotined square. Additionally, some of the strips were visibly bent near their ends. Any adherends with obvious defects were discarded before specimens were bonded. However, this still leaves the possibility of less obvious variations in the end shapes of the adherends. Close examination of the adherends (e.g. the photographs in Figure 12) tends to suggest that there is such a degree of variability in the 'square-ness' and 'flatness' of the guillotined adherends that there is little value in trying to model these exactly.

The decision was taken to remove all adhesive fillets, to leave a square joint end, in order to provide some reproducibility in the bond-end conditions. Excess adhesive fillets were removed using a sharp scalpel with care being taken to avoid damaging the glue line. The procedure appeared to work reasonably well with the softer elastomeric adhesive where fillet removal was easy. Failure loads were reasonably repeatable and the mode of failure – cohesive in the adhesive layer – was the same in all tests. When the fillet is not removed the strength of the specimens increases slightly, as shown in Table 8.

Specimens	**Failure load**	**Failure load/overlap**	**Failure extension**	**Failure strain**
	N	N/mm	mm	
square fillet	585 ± 55	46.3 ± 4.3	0.32 ± 0.05	1.11 ± 0.12
long fillet	648 ± 68	48.8 ± 4.8	0.30 ± 0.07	1.47 ± 0.22

Table 8: Failure results for elastomer lap joint specimens with different fillets at 20 °C and $3x10^{-3}$ s^{-1}

The fillet removal procedure was more difficult for the harder polyurethane adhesive. Failure loads had a large degree of scatter and variable failure modes were observed, including adhesion failure of both the adhesive and primer layers. Damage to the end of the bond line was suspected as a cause of this scatter. It was also observed that some of the specimens tested appeared starved of adhesive. One suspicion was that the high viscosity of the adhesive paste prevented adequate dispersal of the 250 μm diameter glass beads used to control bond line thickness. Thus, there were specimens prepared from adhesive containing no beads. To overcome these problems a second batch of specimens were prepared using 0.5 mm diameter copper wire inserted between the adherends to control bond line thickness. Half of the specimens had their adhesive fillets removed as before (although by a different technician) whilst the remaining specimens were tested with the fillets as bonded.

The results shown in Table 9 indicate that the second batch of PU lap joint specimens, prepared with squared off adhesive fillets, was significantly stronger (by approximately 30 % on average) than the initial batch. Whether this was due to improved bond line thickness control

or to more careful fillet removal is not clear. However, the 'long fillet' specimens are a further 20 % stronger than the specimens where the fillet has been cleaned.

Specimens	Thickness	Failure load/overlap	Failure strain
	mm	N/mm	
Initial batch – square fillet	0.22 ± 0.17	186 ± 49	1.18 ± 0.49
Second batch – square fillet	0.42 ± 0.04	246 ± 54	1.78 ± 0.18
Second batch – long fillet	0.30 ± 0.13	291 ± 38	1.89 ± 0.0.32

Table 9: Failure results for PU lap joint specimens with different fillets at 20 °C and $3x10^{-3}$ s^{-1}

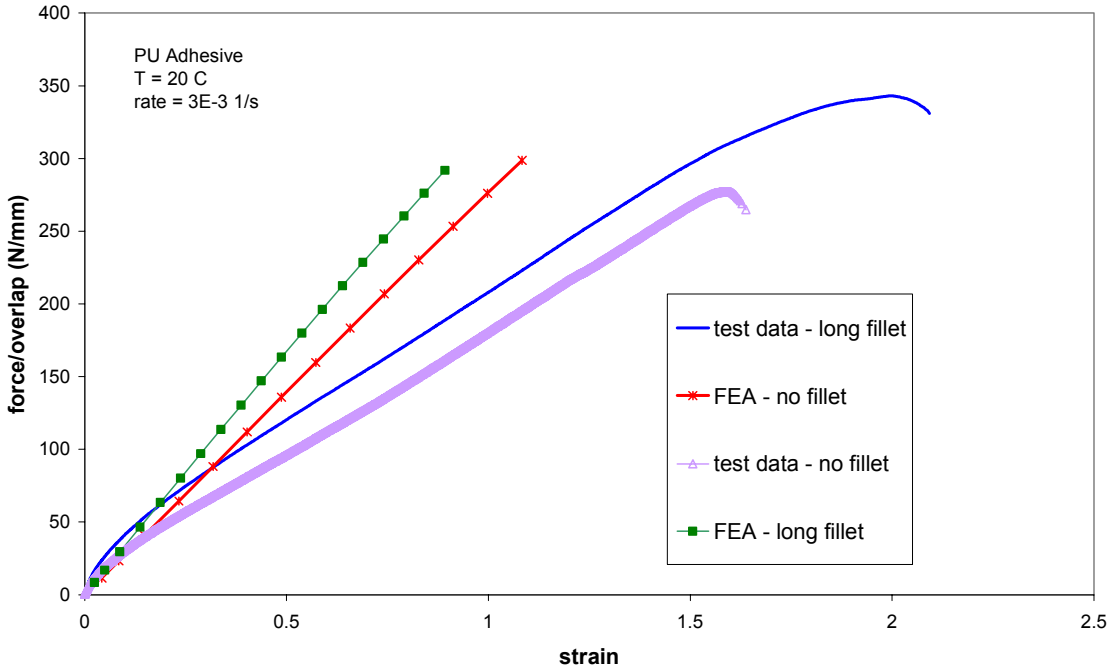

Figure 9: FEA and test data for different types of fillet

A study of the stress-strain curves of the two sets of specimens from the second batch of samples indicates that the specimens retaining fillets are generally slightly stiffer than those whose fillets had been removed (Figure 9). This is probably due to the greater load carrying area (load is carried in part of the fillet protruding beyond the ends of the adherends) and this effect is predicted by the FEA.

Following observations of the specimens manufactured, the lap joint specimen was modelled with a rectangular fillet with a height of 1 mm with lengths varying between 0.25 mm (consistent with a thin layer of adhesive that may be left after removal of the fillet) to 10 mm, whilst maintaining the same size of elements in the adhesive layer by the adherend corners in all the models. Stress analysis of specimens with differing lengths of fillet show that maximum principal stress values are reduced when a fillet is present. However, at the lowest length of fillet (0.25 mm) the stress predictions differ very little from the case where there is no fillet (Figure 10). There seems to be little effect of fillet length for fillets ≥ 1 mm. Plots of the stress distributions (Figure 11) show that the location of the stress concentration shifts from the end of the bond line by the continuous adherend (no fillet) to the corner of the adherend (long

fillet). The major portion of the fillet experiences low stresses and any variation of shape at the ends of the fillet (including changing length) will have insignificant effect on the joint performance. Common fillet shapes are shown in Figure 11

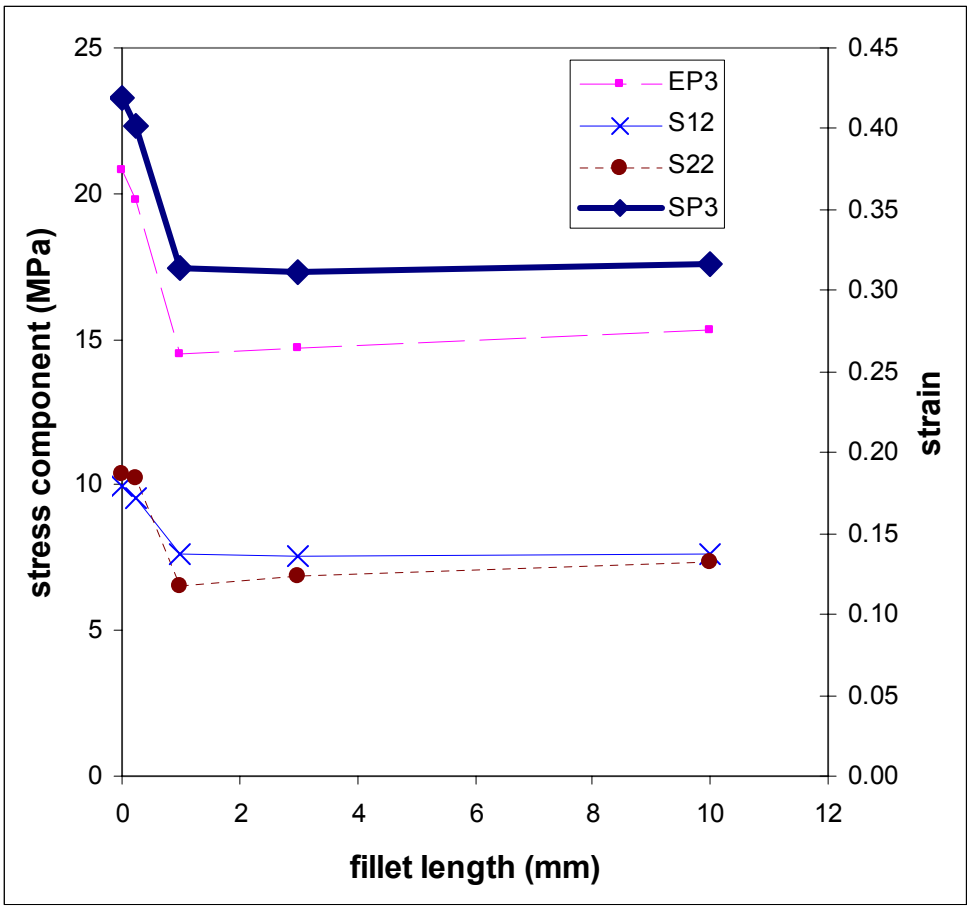

Figure 10: Variation of predicted stress and strain components with fillet length (PU)

3.3.2 Effects of Different Fillet Types

The location of the maximum stress is likely to be near a sharp corner, where the value of the maximum stress depends on the size of the local elements used to model that region, even if a fillet is present. A series of predictions run with a selection of different fillet geometries produced the following conclusions:

- Maximum stress values for any given load are reduced through the presence of a fillet.
- Where there is no fillet or only a very small fillet the stress concentration is located at the end of the bond line where the adhesive attaches to the 'continuous' adherend. (Figure 11a)
    - The predicted maximum stress depends strongly on the element size in this region.
    - Shaping the corners of the adherends gives no benefits in these cases as the stress concentration is not located near the corners.
- Where there is a fillet whose height exceeds the bond line thickness (i.e. one where adhesive 'climbs' the edge of the adherend) the location of stress concentration shifts to the opposite side of the bond line from the corner of the adherend. (Figures 11c and 11d)

- Variations in the shape of a large fillet (rectangular, curved, triangular, etc.) seem to have little effect on either the location or the magnitude of the maximum stress in a joint bonded with a flexible adhesive.
- The stress concentration is highly localised and depends on the size of the elements. However, the dependence on element size is not as significant as for the case where there is no fillet.
- Shaping the adherend corners (e.g. rounding them) affects the stress concentration magnitude and will generally reduce the maximum stress. However, the stress is still localised and values will depend on element sizes although not as significantly as they do for a square corner.

- If the height of the fillet is comparable to the bond line thickness then the location of the stress concentration depends on the geometry of the fillet. (Figure 11b)
  - In the case of short fillets that are curved or triangular the stress concentration moves away from the adherends to the edge of the fillet. Stress concentrations are observed to cover several elements and dependence on element size is assumed to be much reduced.
  - Where the fillets are long the stress concentration predictions are similar to the larger fillet height.

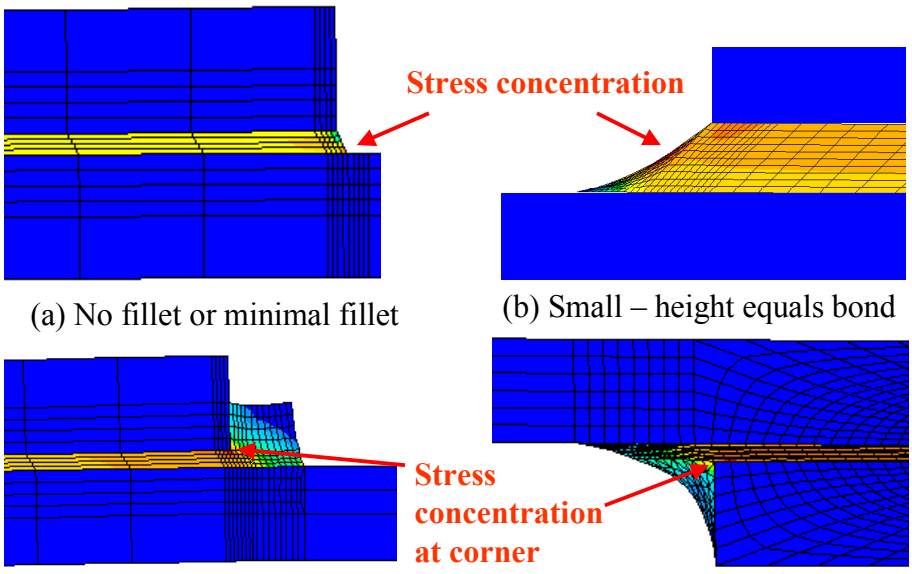

(a) No fillet or minimal fillet

(b) Small – height equals bond

(c) Large fillet – height greater than bond

(d) Small, shaped fillet – height greater than bond

Figure 11: Locations of stress concentrations for different fillet types

3.3.3 Crack Formation and Growth in Fillets

To investigate the initiation and growth of cracks that lead to failure, a series of photographs was taken of a lap joint specimen (with a long fillet). The test was performed at 20 °C and $3x10^{-3}$ s^{-1}. Six photographs are shown in Figure 12 ranging from no load at the start of the test until a point in the test after the maximum-recorded load where the load bearing capacity of the joint is severely reduced. The measured force-extension curve is shown in Figure 13 with the performance predicted by FEA shown for comparison. The loads (and corresponding predicted maximum stress and strain components) for the photographs are summarised in Table 10. The peak load sustained by the specimen (2650 N, equivalent to 201 N/mm of overlap length) is

somewhat less than the average strength of the batch of long fillet samples (291 N/mm). The force-extension response also looks considerably more linear than the 'normal' observed test results.

Photo no.	Load	E12	EP3	S22	S12	SP3	MISES	SENER
	N			MPa	MPa	MPa	MPa	J/mm^3
0	0	0	0	0	0	0	0	0
1	2350	-0.53	0.30	6.27	-7.35	13.81	13.15	2.33
2	2600	-0.58	0.33	6.86	-8.08	15.42	14.59	2.87
3	2650	-0.59	0.34	6.98	-8.24	15.75	14.89	2.99
4	2550	-	-	-	-	-	-	-
5	2500	-	-	-	-	-	-	-
6	2100	-	-	-	-	-	-	-

Table 10: Loads and predicted stress/strain components in the test specimen

In photograph no. 1 (Figure 12) there is indication that a crack has initiated at the corners of the adherends. The presence of a crack is more noticeable at the adherend fillet towards the bottom of the photograph. The crack is observed to grow in subsequent photographs both up through the fillet and round the corner of the adherend into the bond line. However, the crack does not appear to have run very far into the bond line by the time that the maximum load had been reached (photograph no. 3). The drop-off in measured load after the peak is very rapid. By the time the load has dropped to 2100 N (photograph no. 6), fractures are appearing throughout the bond line, indicating a catastrophic loss of load bearing capacity.

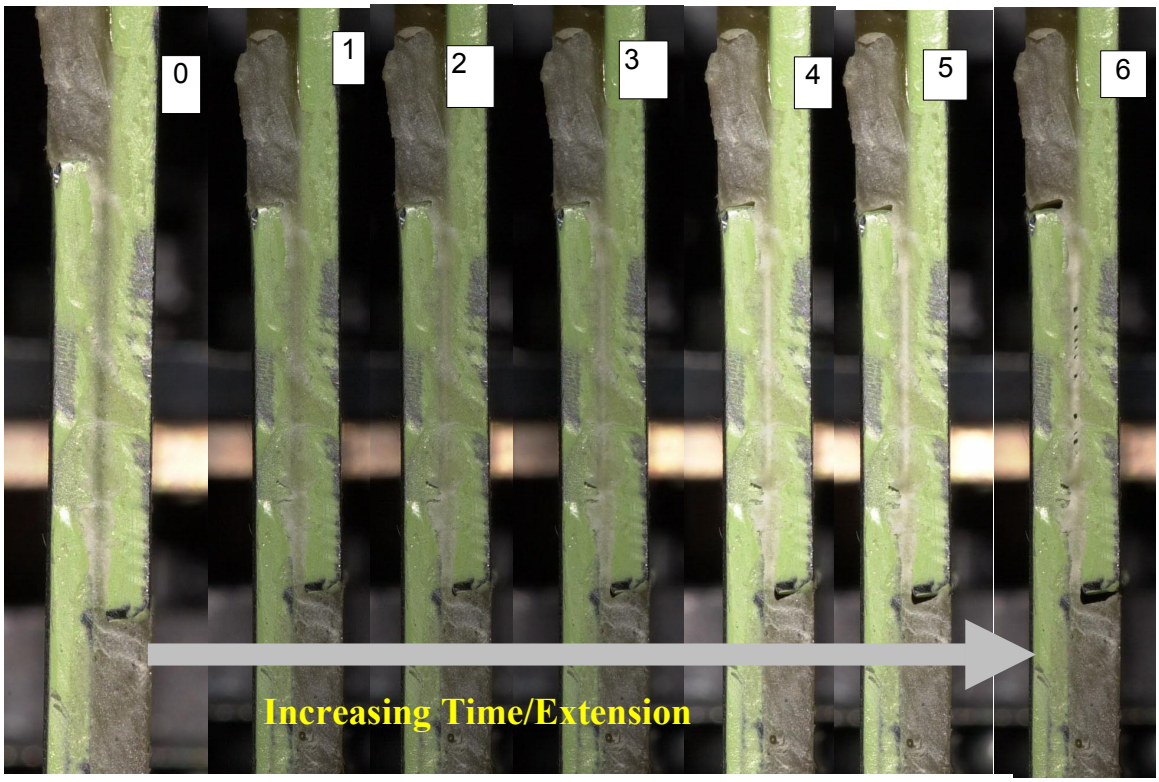

Figure 12: Photographs of a PU lap joint specimen during a test

It is noticeable that the adhesive in the bond line becomes lighter after the maximum load was been reached. This lightening in the colour of the material has been observed in both bulk and

joint specimens. It is ascribed to cavitation or crazing of the material perhaps analogous to the processes that occur during plastic yielding in structural adhesives such as epoxies. However, in the bulk tension tests the whitening of the specimen is not accompanied by any significant softening of the stress-strain response. The whitening of the PU adhesive appears to be a precursor to rupture of the material.

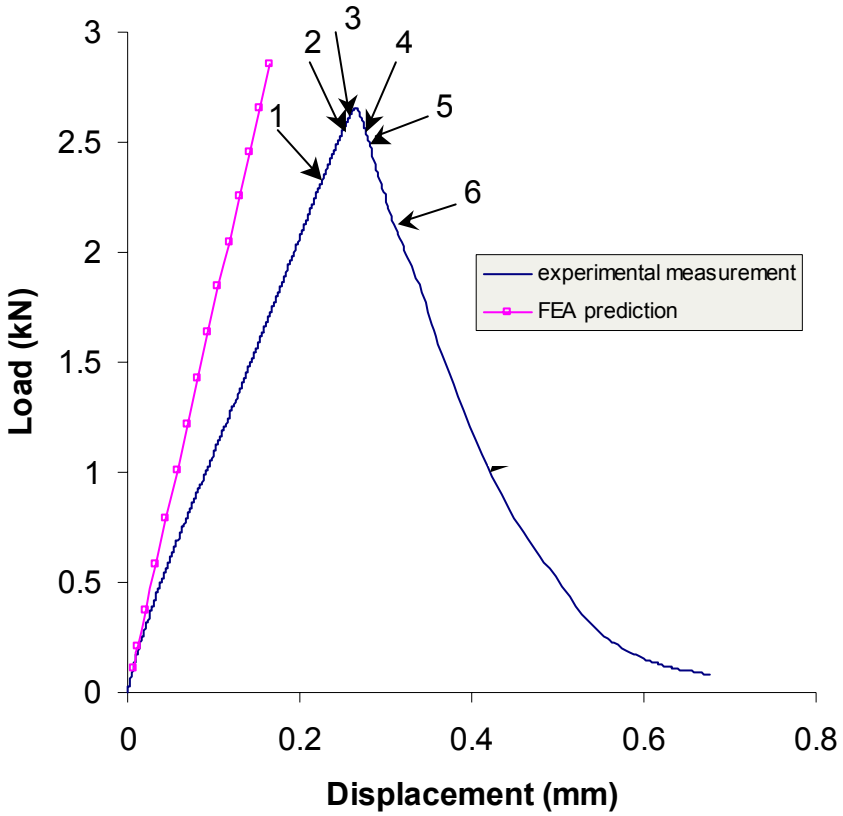

Figure 13: Measured force-extension curve corresponding to photographs in Figure 12

3.4 EFFECT OF JOINT SIZE

The dimensions of the adhesive lap joint (adherend thickness, overlap length, adherend width and bond thickness) will influence the ultimate strength of the lap joint. Broughton [48] reported a study of the influence of parameters for the elastomeric adhesive. A summary of the main effects determined experimentally is given in Table 11.

Adherend Thickness	**Failure Load**	**Bond Length**	**Failure Load**	**Load/Overlap**	**Bond Thickness**	**Failure Load**
mm	N	mm	N	N/mm	mm	N
1.51	1,155	12.5	523 ± 60	41.4 ± 4.8	0.30	1245 ± 207
2.97	1,025	25.0	1,094 ± 109	44.7 ± 4.4	0.50	1368 ± 715
		50.0	1,926 ± 281	38.3 ± 5.6	0.75	1079 ± 523
					1.00	1,014 ± 554

Table 11: Averaged effects of different joint parameters on elastomeric adhesive lap joint failure strength (tested at 20 °C, $3x10^{-3}s^{-1}$)

The failure load is independent of adherend thickness. The adherends are much stiffer than the adhesive and can be considered almost infinitely rigid. There is very little adherend deformation during the tests and so the adherend thickness has an insignificant effect on the stress distribution. The failure load scales with overlap length as expected. The normalised failure load at the longest overlap (50 mm) is slightly lower than the shorter overlaps. It was also noticed that the slope of the measured stress-strain curve tended to decrease with overlap length. The scatter in the data makes it difficult to determine if the bond thickness has any effect on strength. However, the results seem to indicate that the joint strength is at a maximum at 0.5 mm bond thickness. It is noticeable that the strength of the joints is lower than that determined in the study of the effect of rate and temperature summarised in Section 3.1. The reasons for the decline in strength are not known but, speculatively, this could be due to batch-to-batch variability of the material, degradation of the adhesive during storage (stored at 5 °C for several months prior to use) or variations in cure.

FEA was performed for the different overlap lengths and bond thickness values (the adherend thickness was not altered as it has no effect on the results). The predicted SP3 (maximum principal stress) values for the different configurations predicted using a constant number of elements in the bond layer and keeping the same element size at the corner of the adherends, are shown in Table 12. Analyses were run with varying element numbers. These results are shown in Figure 14. The FEA shows the stress concentration growing with increasing bond thickness, with a much more significant effect when the element area is kept constant. The effect of overlap length is less obvious and the interpretation must consider the effect of element size. When the element size is constant, there is a small increase in the predicted peak stress value that seems to correlate with a small reduction in normalised joint strength.

Overlap	thickness,	Constant number of elements, 198 by 8, in bond layer but varying size		Constant size of element, area = 0.000625 mm^2
		Element Area	SP3 variable size	SP3 constant area
mm	mm	mm^2	MPa	MPa
12.5	0.25	0.001973	6.551	7.698
12.5	0.5	0.003946	6.970	9.413
12.5	1	0.007891	7.374	11.600
50	0.25	0.007891	5.563	8.483
50	0.5	0.015783	6.216	10.206
50	1	0.031566	6.874	12.539

Table 12: FEA results for the effect of different elastomeric adhesive joint geometries on predicted maximum principal stress

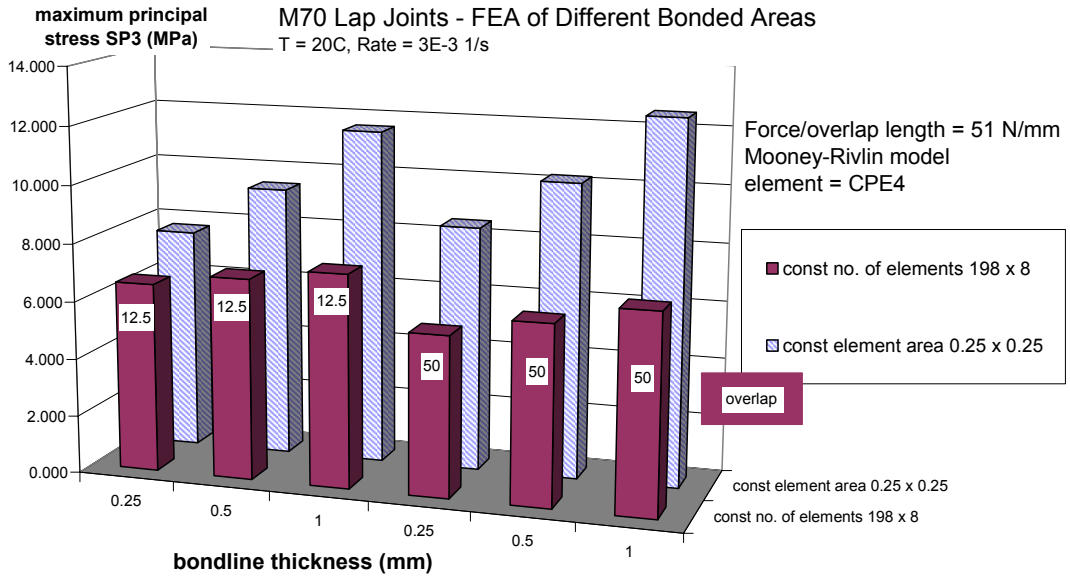

Figure 14: SP3 predictions – effects of overlap, bond thickness and mesh density

3.5 ANALYSIS AT HIGH EXTENSIONS

In the FE models referred to above the stress and strain distributions were calculated at loads comparable to the failure loads determined in the lap joint specimens. However, as the comparisons between measured and predicted force-extension curves show, there is a large difference between the predicted extension and the measured extension. The strains in the joint will be significantly under-estimated. The FE results could have been analysed at extensions comparable to those at failure in the experiments. However, the loads would have been several times those actually measured with the risk that greater deformation or bending of the adherends would be predicted than actually occur (with the resulting risk of distortion of the stress distribution).

Input data	Strain	E12	EP3	S11	S22	S12	SP3	MISES	SENER
				MPa	MPa	MPa	MPa	MPa	J/mm^3
Corrected input (E=7.17 MPa)	1.05	-1.37	0.99	6.10	4.32	-3.61	8.37	6.45	2.85
Standard input (E=11.15 MPa)	0.53	-0.82	0.51	5.08	4.47	-3.16	7.78	5.55	1.28

Table 13: Comparing standard and corrected analyses

As an exercise, the tensile properties of the adhesive were modified to reduce the stiffness of the FE prediction so that it was comparable with the measured data. To achieve this, the slope of the linear portion of the lap shear was calculated to determine a 'shear' modulus (G_L = 2.94 MPa). The corresponding tensile test data were plotted as true stress-against true strain. This plot was roughly linear and the slope taken as the tensile modulus E (11.15 MPa). From E and the Poisson's ratio υ (obtained from the slope of lateral strain against axial strain) the shear modulus (G_T = 4.3 MPa) can be determined:

$$G_T = \frac{E}{2(1+\nu)} \qquad (16)$$

The ratio between G_L and G_T was calculated as 0.6 and used to scale the stress values in the tensile test data down providing a set of input data with a reduced modulus (E = 7.17 MPa) that would produce a predicted slope comparable with the experimental lap joint measurements. The corrected tensile data were reconverted back to engineering stress-strain and stress-volume ratio data and used as input data for an FE analysis of the joint using the Mooney-Rivlin model. The results of the analyses performed using the corrected input data are shown in Figure 15. Generalised plane strain elements (GPE), rather than plane strain (PE) elements, were used to achieve the closest fit to the experimental data. The results of the stress analysis are shown in Table 13 with the predictions from the original dataset added for comparison.

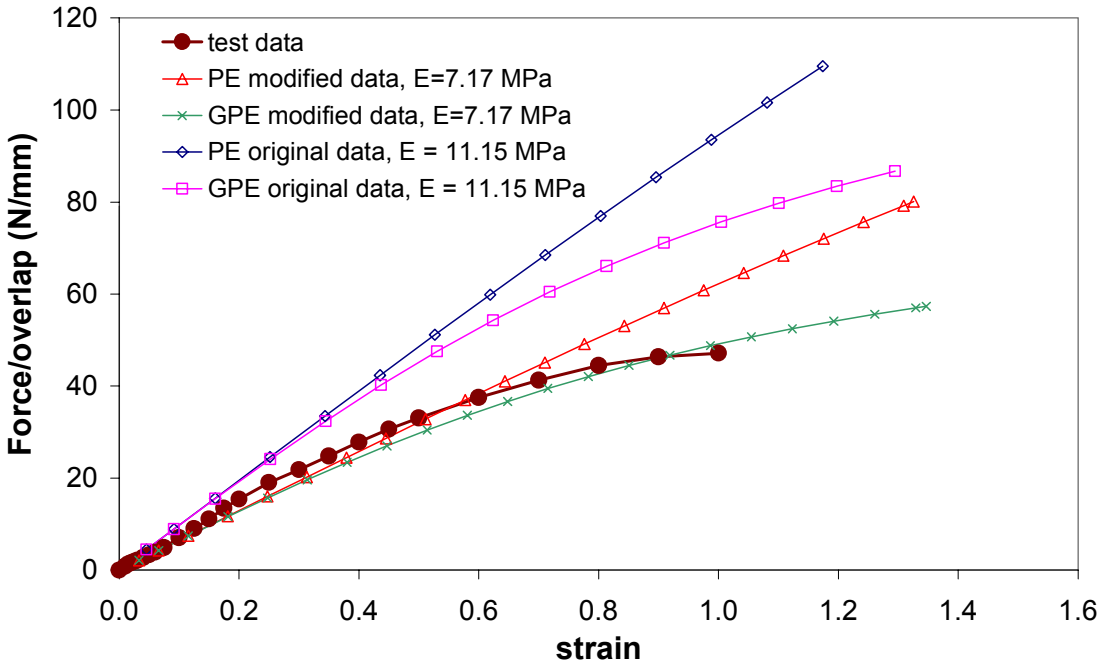

Figure 15: FE analyses with corrected and original tensile data

The modified analysis, run to higher extensions than the standard analysis, predicts much higher strains and strain energies as expected. The differences between the predicted stress values are less significant and for some components, e.g. S22 peel stress, are virtually identical.

These modified data would need to provide accurate predictions of other joint configurations, such as the scarf or the T-peel tests, if this data correction method was to be generally used to improve accuracy of design predictions.

4 SCARF JOINTS

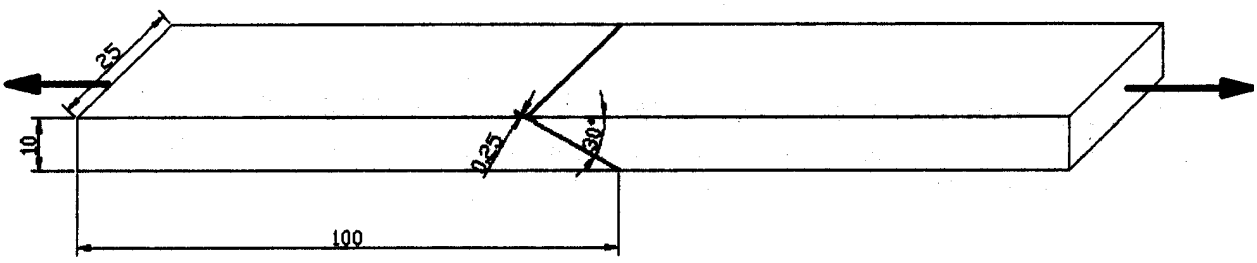

Figure 16: Scarf joint specimen

Scarf joints incorporate a tapered overlap, which is claimed to be beneficial from a basic design viewpoint as peel stress is reduced in relation to shear stress [48, 49]. This arrangement is often used to join thick sections.

By considering the resolution of forces (F) applied to a scarf joint the shear stress σ_S and normal stress σ_{an} in the adhesive layer can be calculated for any taper angle θ [47]:

$$\sigma_S = \frac{P\sin(\theta)\cos(\theta)}{t} \text{ and } \sigma_{an} = \frac{P\sin^2(\theta)}{t} \qquad (17)$$

where P is force per unit width and t is the thickness of the rectangular sections joined. From equation (17), the ratio of σ_S to σ_{an} equals $\tan\theta$ and decreases as the taper angle is reduced.

The scarf joint specimen used in this work is shown in Figure 16. The tapered adherends were made by spark eroding an angled cut, at 30° to the length direction, through rectangular section, 25 mm wide by 10 mm deep, mild steel bars. Two further angular geometries with smaller bonded areas (at 45° and 65° to the length) were also prepared and tested. Specimens were prepared in a special jig to maintain alignment during cure. Most test specimens were prepared with a nominal thickness of 0.5 mm in the length direction (controlled by mixing glass beads, with 0.25 mm diameters, into the adhesive). However, owing to the high viscosity of the adhesive pastes studied, accurate bond line thickness control was difficult to achieve during manufacture. The bond lines of most scarf specimens were measured, using a travelling microscope, to be in excess of 1 mm thick.

Scarf specimens were tested in an Instron 4505 test machine. Specimens were clamped in wedge jaws with care being taken to avoid applying excess force to the specimens when the grips were tightened. Specimen extensions were measured using pairs of knife-edged extensometers (e.g. Instron type 2602) clamped straddling the bond line. The extension of the steel bar was assumed to be negligible during the tests and, therefore, the measured extension

equates to the extension of the bond line. The two extensometers provided a check for specimen bending due to misalignment of specimens or grips. In most cases the two extensometers agreed to within 10 %.

The results for the scarf joint tests carried out at different temperatures and strain rates, for the standard 0.5 mm thick bond, 30° taper angle specimens are shown in Tables 14 and 15. There is considerable scatter in the results that show the expected general trend of increasing load bearing capacity of the joint with increased tensile strength of the adhesive.

In the PU adhesive joint results there was very little reproducibility. In many cases samples run under the same conditions had very dissimilar mechanical responses – there could be a factor of 10 or more between the slopes of the initial linear parts of the force-extension curves. The maximum loads obtained could differ by over 100% of the lowest values. There is sufficient confidence in the testing procedures to conclude that these differences are unlikely to be due to artefacts of the test. The most likely explanation is that these differences are due to specimen preparation.

Temperature	**Strain Rate**	**Load**	**Strain**
°C	s^{-1}	N	
0	$3x10^{-2}$	1395 ± 101	0.28
0	$3x10^{-3}$	956 ± 115	0.13
0	$3x10^{-4}$	893 ± 101	0.10
20	$3x10^{-2}$	824 ± 232	0.18
20	$3x10^{-3}$	802 ± 134	0.26
20	$3x10^{-4}$	690 ± 132	0.20
40	$3x10^{-2}$	693 ± 118	0.14
40	$3x10^{-3}$	691 ± 47	0.28
40	$3x10^{-4}$	599 ± 66	0.23

Table 14: 30° scarf joint bonded with the elastomeric adhesive

Temp	**Rate**	**Force**	**Strain**	**Maximum Force**
°C	s^{-1}	N		N
0	$3x10^{-3}$	>5500	>0.02	*
20	$3x10^{-4}$	2757 ± 856	0.337 ± 0.103	3362
20	$3x10^{-3}$	3727 ± 90	0.308 ± 0.089	3790
20	$3x10^{-2}$	3896 ± 2315	0.295 ± 0.058	5533
40	$3x10^{-3}$	771 ± 357	0.164 ± 0.037	1601

Table 15: 30° scarf joint bonded with PU adhesive

*Note: *Specimen was not broken within capacity of the 5kN load cell. Material is in the rigid, glassy state so further testing or analyses were not performed.*

It was difficult to control bond line thickness when manufacturing test specimens. Prior to testing, bond line thickness was measured at both exposed edges of the bond using a travelling microscope. Although the presence of un-removed adhesive flash at the edges of the bonds could make it difficult to precisely determine the adherend-adhesive interface, there was a tendency for the two averages of the thickness values to differ by up to 25 %. Whether these differences are due to difficulty in aligning specimens during cure or to adherend faces not being cut exactly parallel in the through-thickness direction is not known. However, there did

not seem to be any correlation between differences in width and strength/stiffness results obtained from the limited number of tests performed.

Poor adhesion might also lead to differences in the test results but visual observations of the failed specimens did not indicate any consistent differences in failure mode. The scale of the variations would suggest that, for some specimens, less than 50 % of the joint was bearing load. The failure surfaces tend not to support this. The most likely explanation for the differences is variation of the mix ratios of the adhesive in the bond line. Where a large amount of adhesive was dispensed and then transferred to the surfaces of the adherends using a spatula (as for the specimens tested at 20 °C and 3 x 10^{-3} s^{-1}) the results were consistent. Where material was dispensed directly onto the adherends from the cartridges via the mixing nozzle the results were extremely inconsistent. It is believed that the cyclic application and release of pressure on the adhesive when dispensing small quantities to make the specimens leads to unequal flow of the components into the nozzle. Thus, some specimens may have contained adhesive with the wrong mix ratio, which would not have cured to the optimum level and thus have a lower modulus and strength. Due to the large variation in measured joint performance, all analyses of the PU scarf behaviour were made relating to the specimens where maximum strength was obtained.

4.2 FE MODELLING OF SCARF JOINT

A typical mesh and boundary condition configuration for a scarf joint analysis is shown in Figure 17. The adhesive layers in the scarf joints were modelled using 2-dimensional plane strain (PE), 2-dimensional generalised plane strain (GPE) and 3-dimensional 'brick' elements (3D). Both triangular (e.g. CPE3, CGPE5) and quadilateral elements were used in the 2-dimensional models. In most of the analyses performed the glue layer was meshed with 32 divisions along the diagonal length and 4 divisions across the glue layer. The number of elements and number of nodes in each element had negligible effect on the force-extension predictions. The GPE predictions showed curvature most like the experimental measurements but the PE predictions are closest to the 3D predictions.

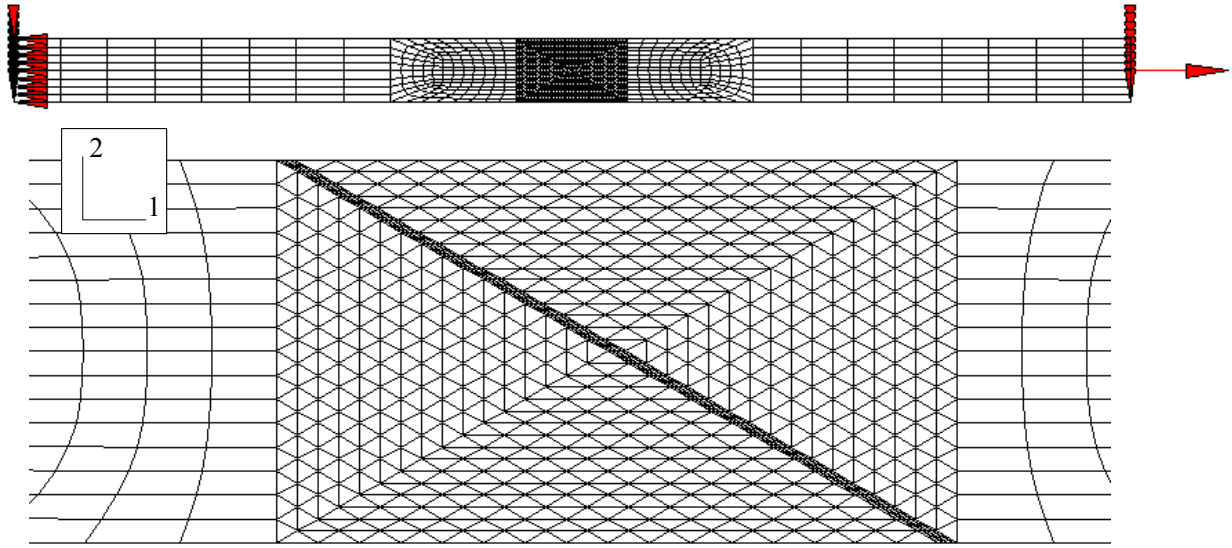

Figure 17: FE mesh for 30° scarf specimen

The results of stress analyses for the 'standard' 30° scarf specimen with a 0.5 mm bond thickness are shown in Tables 16 and 17. The predominant stress is tensile (S11) with shear stress components much less significant. The Mises stress values are comparable with the SP3

values. The strain (extension/thickness) at maximum load in the predictions is comparable to the measured values in the tests.

Temp	Rate	Load	Strain	E11	E12	EP3	S11	S12	SP3	MISES	SENER
°C	s^{-1}	N					MPa	MPa	MPa	MPa	J/mm^3
40	$3x10^{-4}$	599	0.24	0.16	0.14	0.17	2.03	0.46	2.13	1.96	0.20
40	$3x10^{-3}$	691	0.25	0.17	0.15	0.19	2.43	0.51	2.53	2.26	0.24
40	$3x10^{-2}$	693	0.31	0.15	0.13	0.16	2.33	0.55	2.45	2.29	0.22
20	$3x10^{-4}$	690	0.23	0.16	0.14	0.18	2.40	0.52	2.50	2.26	0.24
20	$3x10^{-3}$	802	0.29	0.18	0.15	0.19	2.83	0.58	2.94	2.64	0.30
20	$3x10^{-2}$	824	0.27	0.14	0.13	0.16	2.71	0.68	2.84	2.75	0.26
0	$3x10^{-4}$	893	0.24	0.19	0.16	0.20	3.09	0.66	3.20	2.95	0.35
0	$3x10^{-3}$	956	0.28	0.15	0.15	0.17	3.15	0.79	3.30	3.20	0.32
0	$3x10^{-2}$	1395	0.26	0.15	0.14	0.16	3.65	1.20	4.71	4.72	0.45

Table 16: Stress analysis results for elastomer scarf joint

Temp	Rate	Load	Strain	E11	E12	EP3	S11	S12	SP3	MISES	SENER
°C	s^{-1}	N					MPa	MPa	MPa	MPa	J/mm^3
20	$3x10^{-4}$	3360	0.26	0.32	0.19	0.34	12.38	2.04	12.69	11.48	2.12
20	$3x10^{-3}$	3790	0.23	0.31	1.77	0.33	15.85	2.47	15.70	13.50	2.56
20	$3x10^{-2}$	5530	0.14	0.17	0.16	0.19	17.44	4.85	18.41	19.09	2.07
40	$3x10^{-3}$	1600	0.15	0.19	0.15	0.20	5.59	1.16	5.79	5.39	0.68

Table 17: Stress analysis results for PU scarf joint

4.3 EFFECT OF SCARF ANGLE

The effects of scarf angle on the mechanical performance of elastomer joints were assessed using three different angles - 65°, 45° and 30° (the standard angle of the specimens described above). Taking advantage of existing adherends, these specimens were made from bars of cross-section 10 mm deep by 15 mm wide. These were tested at 20 °C and 3 $x10^{-3}$ s^{-1} strain rate. Some specimens 25 mm wide with a 45° taper were also bonded and tested. The results of these tests are shown in Table 18.

Specimen width	Scarf Angle	Failure Load	Load/Unit Bonded Area	Analytical Shear Stress	Analytical Normal Stress	Maximum Principal Stress	Mises Stress
mm		N	N/mm^2	MPa	MPa	MPa	MPa
15	65°	203 ± 50	1.22 ± 0.30	0.52	1.11	1.51	1.04
15	45°	271 ± 32	1.28 ± 0.15	0.90	0.90	1.75	1.27
15	30°	353 ± 37	1.18 ± 0.12	1.01	0.59	2.31	1.95
25	45°	571 ± 59	1.62 ± 0.17	1.14	1.14	2.26	1.63
25	30°	802 ± 134	1.60 ± 0.27	1.39	0.80	2.94	2.64

Table 18 Effect of scarf angle on joint properties

It is to be expected that the failure loads should be 60% of those of the 25 mm wide specimens tested under the same conditions. However, the average load at failure of the 15 mm wide 30° specimens (353 ± 37 N) is considerably lower than 480 N, which is 60% of the average failure

load of the 25 mm wide 30° specimens (802 ± 134 N). Similarly, the 15 mm wide 45° specimen (271 ± 32 N) is not as strong as would be expected from the 25 mm wide specimen results (predicted to be 343 N). The thinner scarf joint specimens were observed to be slightly 'tacky' to the touch, which provides the suspicion that these samples were under-cured in comparison to the 25 mm samples. The under-curing probably resulted from using a different, larger jig, that took longer to heat to temperature, to align the samples during cure but maintaining the same cure schedule as used for the samples that were 25 mm wide. Therefore, the material properties determined from bulk specimens to model the adhesive layer will not accurately represent the properties of the adhesives in these specimens. The results, however, still allow some conclusions to be made regarding effects of changing the geometry of the test specimen.

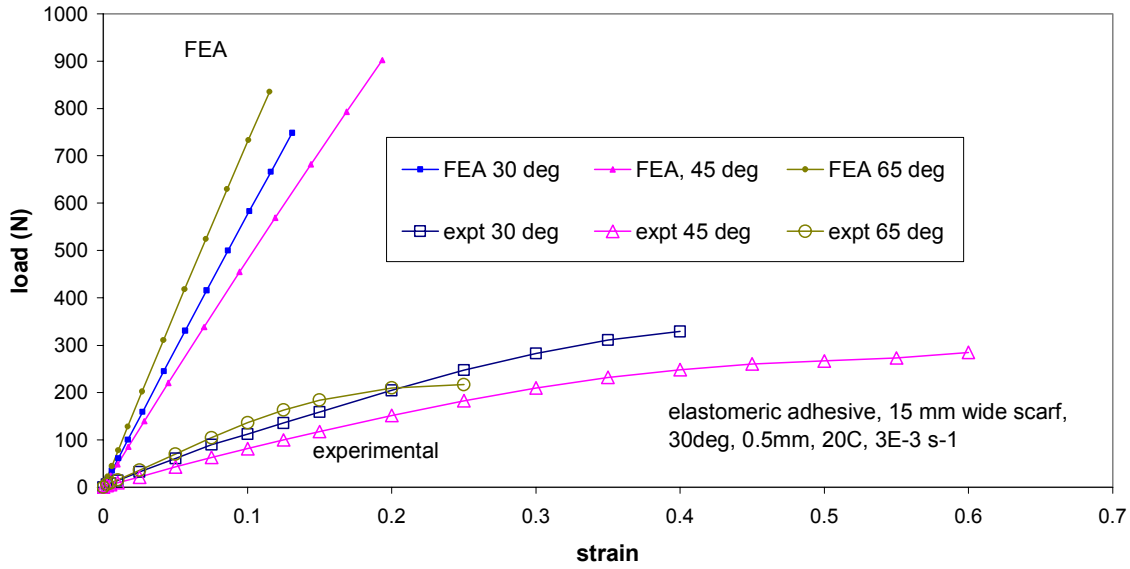

Figure 18: Comparison of measured and predicted force extension responses for different scarf angles

The predicted results show that as the taper angle decreases the strength of the joint increases. This could be attributed to a change in the balance between average shear and normal stress in the specimen as calculated using Equation 17 and seems to be the case as the highest predicted normal stress values occur at the steeper angles where joint strength is lower. However, FEA predicts that the main load transfer mechanism across the bond line is tensile stress in the direction of loading (this is nearly equal to the maximum principal stress). As the results of FEA analysis show the peak value in the maximum principal stress (much like the von Mises and other stress components) at failure follows an opposite trend to the normal stress values. For each width of joint tested the value of the failure load per unit of bonded area is remarkably constant with scarf angle within the bounds of the uncertainties.

The FE stress analysis results show that tensile stress (S11), virtually identical to the maximum principal stress, is the highest stress component in each of the scarf joint configurations. This contrasts with the analytical analyses that show normal stress components becoming more significant as the scarf angle increases. It should be recognised that the analytical and FEA models use different reference axes so that the results are not directly comparable. There is little consistency between maximum stress levels predicted in the adhesive at the failure load.

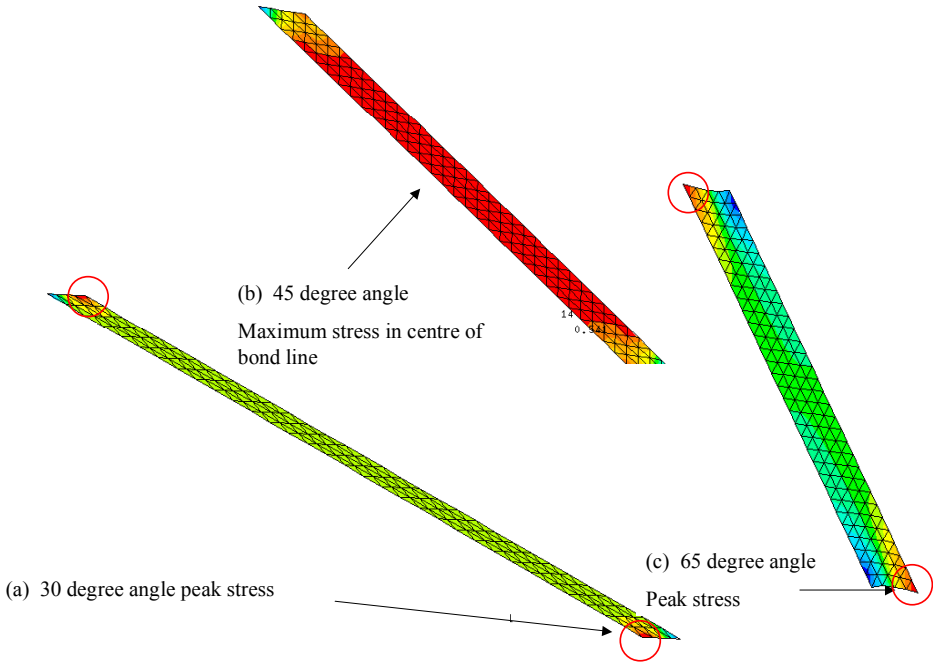

Figure 19: Location of stress concentrations in scarf joint specimens

The changing scarf angle influences the predicted stiffness of the scarf joint specimens (Figure 18). This is lowest at the 45° scarf angle and highest at 65°. This trend is reflected in the experimental results. However, owing to the different cure state of the 15 mm wide scarf specimens, the FEA significantly overestimates the stiffness of the joints. A further effect of changing the scarf angle is to alter the locations on the stress concentrations (Figure 19). At 30° all of the stress and strain components are at a maximum at the end of the bond line by the 'points' in the adherends. At the steeper angles, many of the stress concentrations vanish with the peak stress region covering a major portion of the centre of the glue line. Where stress components (such as the Mises and Tresca stresses) and strain components that do show concentrations at the end of the bond line, these occur opposite the sharp corner of the adherend.

4.4 CRACK INITIATION IN SCARF JOINTS

Photographs were taken of a 30°-angle PU scarf joint that was tested at 20 °C and $3x10^{-3}$ s^{-1}. These are shown in Figure 20 and the corresponding test data in Figure 21. Table 19 contains information on the loads corresponding to each photograph and the stress and strain components predicted by FEA. The failure initiates at the edge of the bond by the 'point' of the adherend (photo 2). It then grows across to the opposite side of the bond (photos 3 - 5) before running along the interface (photos 6 – 8). At the point of maximum load, the crack has run along a significant length of the interface (photo 6).

The shape of the measured force-extension curve is somewhat atypical of the general curves measured for PU scarf joints. The 'kink' in the curve around 1200 N is unusual and there is no obvious cause. There was no sign of cracking before this kink (photo 1) and, although cracks had appeared after this (photo 2), it is unlikely that material failure plays much of a role in the sudden change in stiffness. There is some evidence that there is stress whitening around the ends of the bond and the start of a crack after the kink (photo 2). However, this photo was taken at a load significantly above the kink. The ultimate load on the joint (2126 N) is

considerably lower than the assumed strength of the scarf joint under these test conditions (3790 N).

Photo	Load	E11	E12	EP3	S11	S22	S12	SP3	MISES	SENER
	N				MPa	MPa	MPa	MPa	MPa	J/mm^3
1	1000	0.10	0.13	0.10	4.68	2.17	1.68	4.67	4.91	0.10
2	1500	0.16	0.17	0.16	7.43	3.40	2.17	7.44	7.59	0.88
3	1800	0.20	0.19	0.20	9.09	4.15	2.46	9.10	9.20	1.35
4	1900	0.21	0.20	0.21	9.64	4.39	2.56	9.65	9.74	1.50
5	2000	0.22	0.21	0.22	10.19	4.64	2.65	10.20	10.27	1.66
6	2126	0.24	0.22	0.24	10.88	4.95	2.78	10.90	10.95	1.85
7	1750									
8	End of test									

Table 20: Loads and FEA results corresponding to scarf photos (Figure 20)

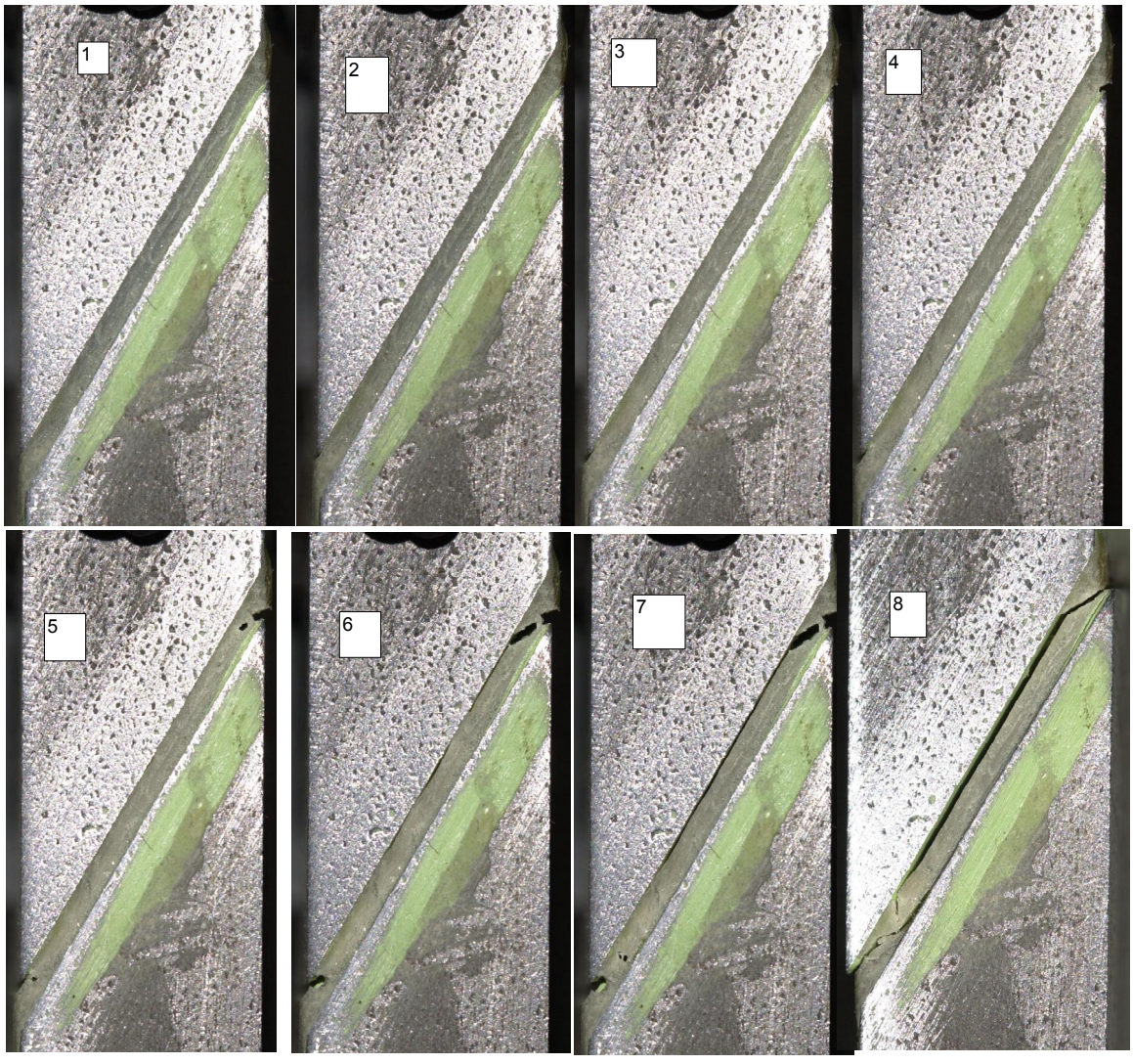

Figure 20: Crack initiation and growth in a scarf joint test (PU adhesive)

The image analysis of the photographs also suggests that, in addition to the applied displacement in the downward direction, the lower adherend also moves to the left. This is consistent with the FEA predictions of a force in the 2-direction equivalent to around 10 % of the applied force in the 1-direction. The FE model does not allow for any compliance of the test machine. However, a small displacement of the adherend is predicted in the 2-direction close to the bond line, thought to be due to elastic bending of the adherend.

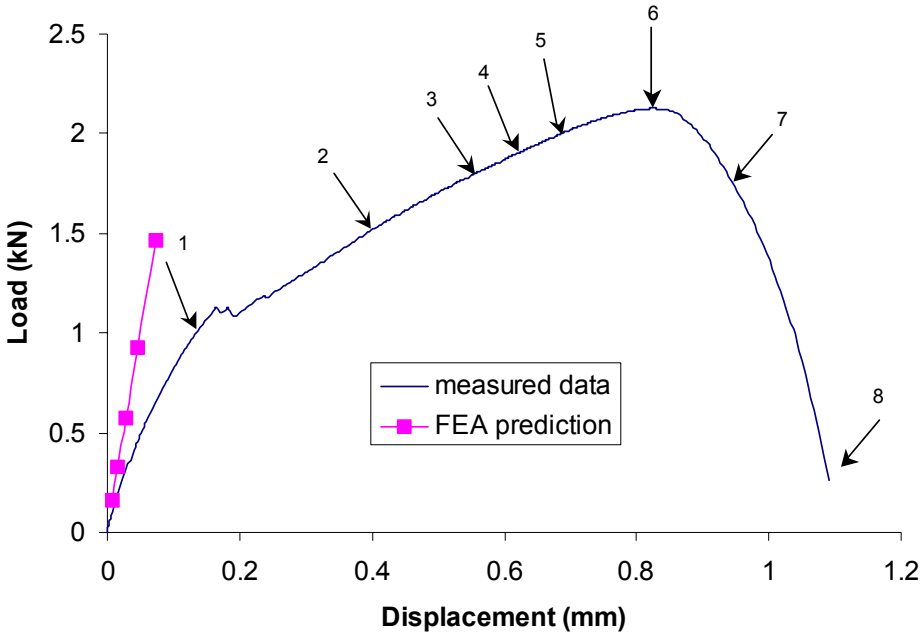

Figure 21: Force-extension response of scarf test corresponding to photographs in Figure 20

4.5 EFFECT OF BOND THICKNESS

The thickness of the adhesive bond line also influences the predicted performance of the scarf joint. The scarf joints tested were between 0.5 and 1 mm thick in the axial direction. FEA simulations were performed at different bond line thickness values. The predicted stiffness normalised by the bond line thickness appears to be independent of thickness – predicted force-strain plots almost directly overlay each other and average stress values in the centre of the bond line are almost independent of bond thickness. There is little evidence of any direct correlation between bond line thickness and normalised stiffness in the experimental results. Table 21 suggests that increasing the thickness of the adhesive layer leads to higher stress concentrations at the ends of the adhesive bond line. This suggests that the strength of the scarf joint should decrease with increasing thickness. This would appear to occur (e.g. Figure 22) although scatter in the results prevents definitive conclusions from being drawn.

Adhesive	**Bond Thickness**	**Failure Load**	**Peak Maximum Principal Stress**	**Average Shear Stress**	**Average Maximum Principal Stress**	**Analytical Shear Stress**	**Analytical Normal Stress**
	mm	N	MPa	MPa	MPa	MPa	MPa
Elastomer	0.5	802	2.94	0.56	2.36	1.39	0.80
Elastomer	1.0	802	3.28	0.55	2.36	1.39	0.80
Elastomer	1.5	802	4.17	0.53	2.41	1.39	0.80
Elastomer	2.0	802	4.45	0.53	2.42	1.39	0.80
PU	0.5	3750	13.7	2.42	11.2	6.50	3.75
PU	1.0	3750	15.6	2.41	11.3	6.50	3.75

Table 21: Effects of bond line thickness on predicted scarf joint stress concentrations (elastomeric adhesive)

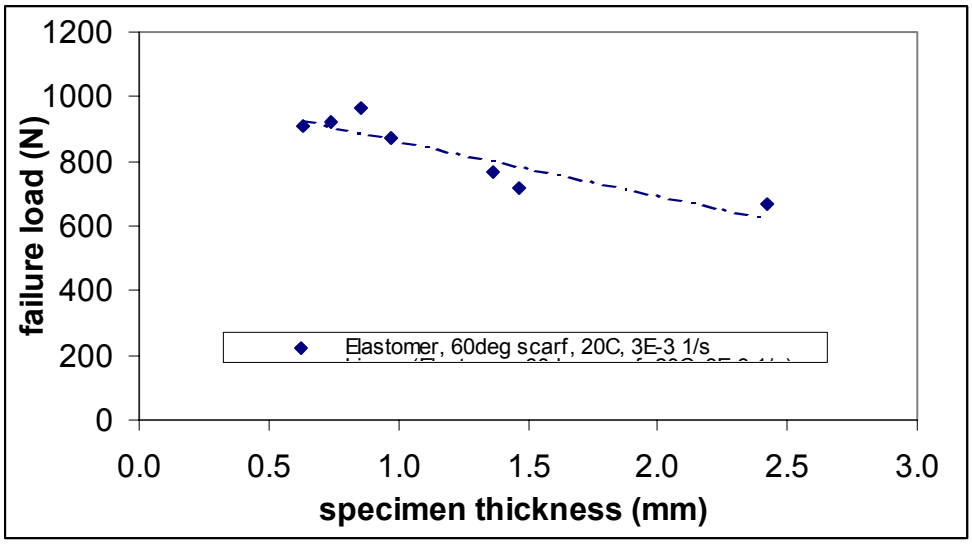

Figure 22: Effect of bond line thickness on elastomeric adhesive scarf joint strength

5. T-PEEL JOINTS

5.1 T-PEEL EXPERIMENTS

The T-peel test [50-54] is a commonly used test with the primary purpose of determining the relative peel resistance of adhesive bonds between flexible adhesives. Since the deformation of the adherends is significant the test cannot be used to determine design data or material properties. However, it is widely used for ranking systems in industry, particularly for assessing the durability of adhesive joints, since it is easy to perform and the configuration resembles in-service bonding problems. The flexible adhesives are peeled at 180° to each other in a tensile test machine. The results should show the load increasing to a maximum and then dropping to a plateau force as the adherends are peeled apart. The initial part of the force-extension trace is ignored and the average plateau force is determined as the peel strength. This test has been shown to discriminate between different combinations of adhesive and pre-treatments however the scatter in results can be high [52, 54]. However, Broughton *et al* [55] have suggested that the peeling force can be relatively insensitive to some modes of degradation and that the peak force may be more sensitive.

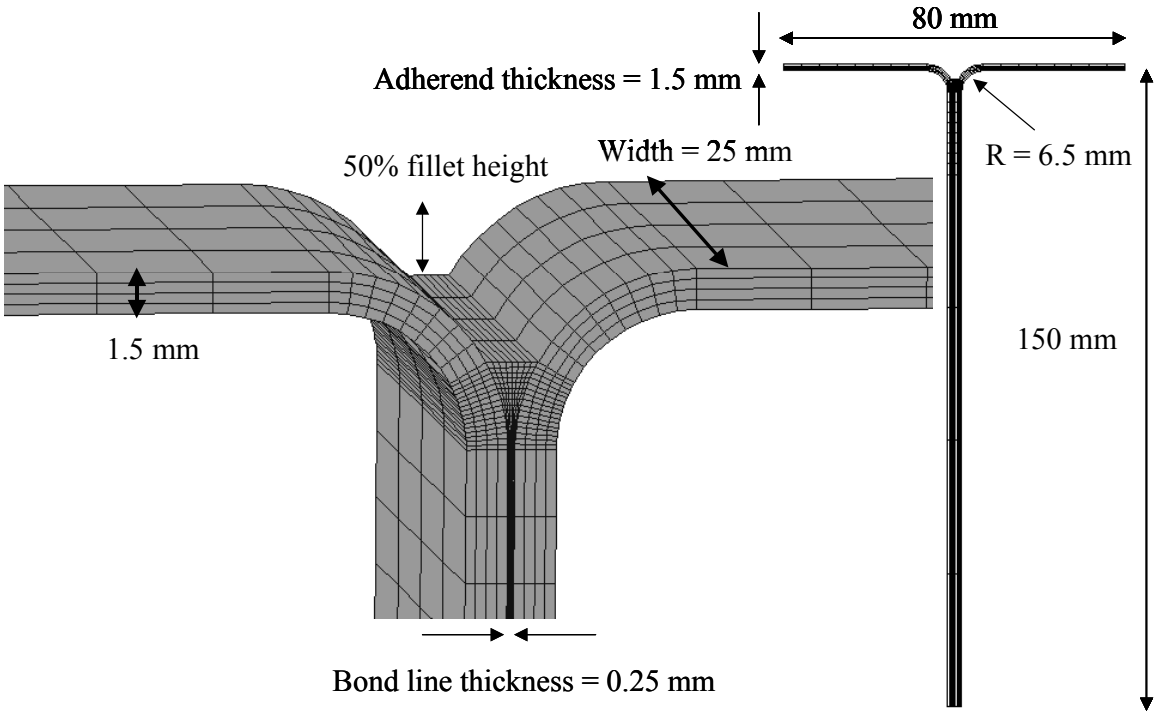

Figure 23: T-peel test specimen

Adherends for the T-Peel test specimen were manufactured from mild steel strips with a 25 by 1.5 mm cross-section by bending through 90° to obtain a radius of curvature of 6.5 mm. These shaped adherends were bonded together along the long 'arms' of the specimen as shown in Figure 3. Specimens were bonded in a jig to maintain alignment during cure. The bond line thickness was controlled at a nominal 0.25 mm by mixing ca. 1 % by weight of 250 μm diameter glass beads in with the adhesive. The fillet at the end of the joint was 50% of the height of the curved section of the joint. This was made by using a shaped tool to scrape off excess adhesive [55]. The T-peel specimen geometry is shown in Figure 23.

The T-Peel specimens were tested in an Instron 4505 test machine. The extension across the bond line was measured using a video extensometer with gauge marks separated by 25 mm. The bond line thickness was determined by subtracting the adherend thickness from the total thickness measured for the bonded arm of the specimen. For each specimen small extension tests were used to set the test speed so that the ratio of measured extension rate to bond line thickness equalled one of the three standard strain rates used in this work ($3x10^{-2}$, $3x10^{-3}$ or $3x10^{-4}$ s^{-1}).

The T-Peel test results for both flexible adhesives followed similar trends. The load climbed rapidly to a maximum and then slowly fell off as the crack propagated along the specimen. The load diminished continually throughout the test and never stabilised to give a region where a 'peel strength' could be determined. Since this region would be governed by fracture behaviour it is of little relevance to understanding the continuum behaviour of the adhesives. At the relatively slow strain rates investigated the times taken to peel a significant length of the specimen were high in relation to the time taken to reach maximum load and the extra data obtained after the maximum were not thought particularly useful. Therefore, the majority of the tests were terminated soon after the maximum load had been reached.

The loads quoted in Tables 22 and 23 represent the maximum loads measured in the T-peel tests. They are not 'peel strengths' as specified in the standards [50, 51].

Temp	**rate**	**thickness**	**Load**	**extension**	**ext/thickness**
°C	s^{-1}	mm	N	mm	
0	$3x10^{-2}$	0.50	514 ± 20	0.55 ± 0.10	1.10 ± 0.20
20	$3x10^{-2}$	0.62	389 ± 9	0.46 ± 0.02	0.73 ± 0.07
20	$3x10^{-3}$	0.43	350 ± 16	0.47 ± 0.02	1.13 ± 0.32
20	$3x10^{-4}$	0.62	307 ± 9	0.43 ± 0.01	0.71 ± 0.08
40	$3x10^{-2}$	0.60	328 ± 18	0.42 ± 0.03	0.70 ± 0.06

Table 22: T-peel results for elastomeric adhesive

Temp	**rate**	**thickness**	**Load**	**extension**	**ext/thickness**
°C	s^{-1}	mm	N	mm	
40	$3.4\ x10^{-2}$	0.44 ± 0.11	678 ± 48	0.31 ± 0.03	0.73 ± 0.16
20	$2.6\ x10^{-2}$	0.35 ± 0.08	1264 ± 206	0.80 ± 0.10	2.53 ± 0.88
20	$2.8\ x10^{-3}$	0.32 ± 0.02	937 ± 154	0.54 ± 0.19	1.69 ± 0.48
20	$3.2\ x10^{-4}$	0.34 ± 0.06	758 ± 143	0.44 ± 0.01	1.30 ± 0.20
0	$3.0\ x10^{-2}$	0.40 ± 0.03	1424 ± 109	0.15 ± 0.03	0.39 ± 0.14

Table 23: T-peel results for PU adhesive

5.2 FE MODELLING OF T-PEEL

Figure 22 shows the mesh used for the end of the T-peel specimen and the overall dimensions of the test piece. The T-peel test was modelled using both 2- and 3-dimensional models. General comparisons of predicted and measured T-peel behaviour indicate that the predictions are much more linear than measurements. The 2-dimensional model predictions are stiffer than the 3-dimensional models, which are closer to the experimental results (Figure 24). In all cases the specimen 'softens' considerably more than the FE predictions and the measured extension at the maximum load is much greater than predicted. It is possible that the adhesive

ruptures early in the test and the slow growth of a crack is responsible for the observed softening.

FE Analyses of the T-Peel specimen indicates that the location of the maximums in the stress and strain distributions occur away from the end of the adhesive fillet at the point where the arms of the specimen start to curve out (Figure 25). This is in contrast to other reported analyses of structural adhesives [54] where peak stresses were predicted to occur at the ends of the fillets. The region of maximum stress covers several elements, indicating low sensitivity of predictions to element size. Results from analyses, at constant loads, performed with differing mesh densities showed that the maximum values for stress and strain components in the adhesive layer were reasonably independent of element size. The T-peel adherends deform significantly during the test and the plastic yielding of the steel adherends is likely to influence the results. Examination of the stress in the adherends shows that some regions will yield before the maximum loads are reached.

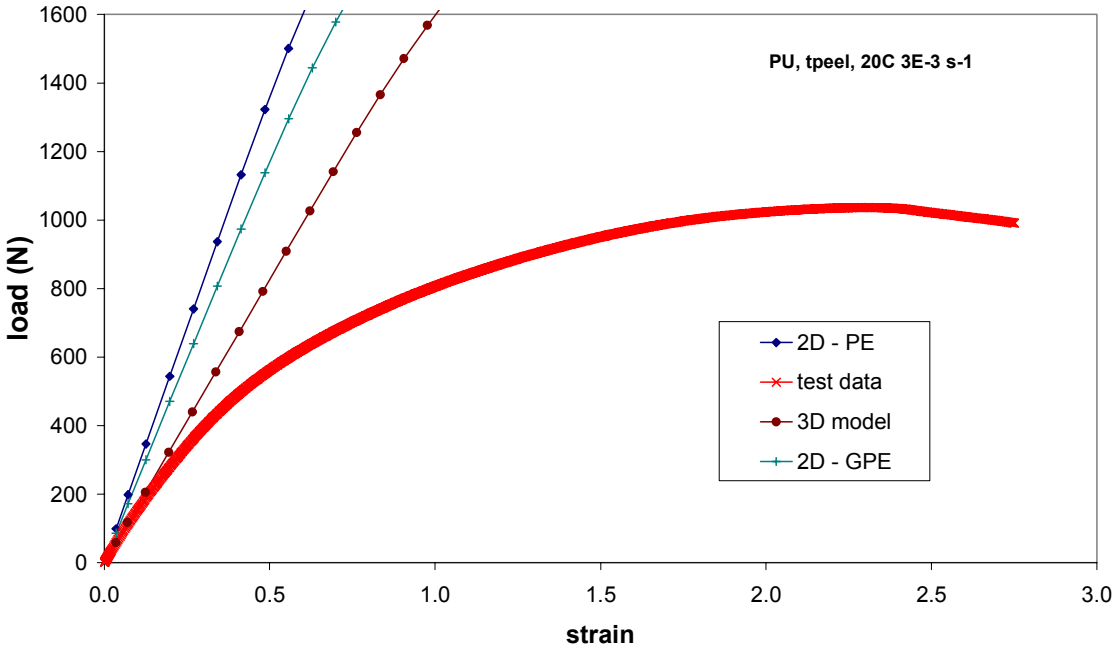

Figure 24: Effect of element type on T-peel force-extension predictions (PU)

Temp	rate	Load	Ext/thickness	EP3	S12	SP3	MISES	SENER
°C	s^{-1}	N			MPa	MPa	MPa	J/mm^3
0°C	$3x10^{-2}$	514	0.32	0.108	1.03	6.97	2.57	0.32
20°C	$3x10^{-2}$	389	0.29	0.110	0.70	4.78	1.62	0.21
20°C	$3x10^{-3}$	350	0.26	0.118	0.67	4.53	1.43	0.17
20°C	$3x10^{-4}$	307	0.27	0.111	0.57	3.91	1.23	0.15
40°C	$3x10^{-2}$	328	0.26	0.112	0.61	4.15	1.34	0.17

Table 24: T-peel results for elastomeric adhesive

Temp	rate	Load	ext/thickness	EP3	SP3	MISES	SENER
°C	s^{-1}	N			MPa	MPa	J/mm^3
40	$3x10^{-2}$	678	0.57	0.122	10.33	2.58	0.52
20	$3x10^{-2}$	1264	0.61	0.105	22.43	7.18	1.07
20	$3x10^{-3}$	937	0.57	0.177	20.02	5.36	1.48
20	$3x10^{-4}$	758	0.3	0.123	11.76	3.03	0.65
0	$3x10^{-2}$	1424	0.28	0.017	48.09	40.33	0.29

Table 25: T-peel results for PU adhesive

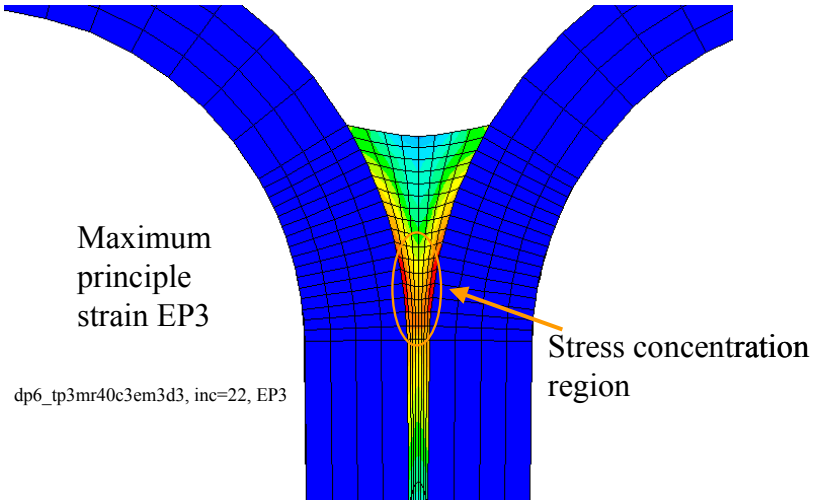

Figure 25: Stress/strain distribution in T-peel specimen

5.3 EFFECT OF BOND THICKNESS

T-peel specimens were prepared with a nominal adhesive layer thickness of 0.25 mm. However, this was difficult to control and, although, within specimens, the bond thickness tended to be constant along the length of the specimen, measured thickness values ranged from 0.25 mm to 0.6 mm. FE models were run assuming 0.25 mm and 0.5 mm thick bond lines. The thicker bond line gives a lower stiffness response and is closer to the measured data. The results of the stress analysis vary with thickness. These are summarised in Table 26 below.

Temp	Rate	Load	E12	EP3	S11	S22	S12	SP3	MISES	SENER
°C	s^{-1}	N			MPa	MPa	MPa	MPa	MPa	J/mm^3
40	$3x10^{-2}$	678	0.14	0.12	7.88	6.53	1.23	7.94	2.81	0.32
20	$3x10^{-4}$	758	0.14	0.12	8.99	7.36	1.44	9.06	3.31	0.42
20	$3x10^{-3}$	937	0.14	0.12	11.46	9.19	1.84	11.50	4.37	0.57
20	$3x10^{-2}$	1264	0.09	0.09	17.39	12.72	2.90	17.42	8.30	0.78

Table 26: FEA stress and strain components for 0.5 mm thick PU T-peel bond

The effect of increasing the thickness of the adhesive layer in the T-peel tests appears to be reductions in the stress and strain concentrations in the adhesive layer. This suggests that the peel strength ought to increase with bond thickness.

5.4 FAILURE MODE OF T-PEEL SPECIMENS

The location of the stress concentration, away from the end of the fillet, differs from the locations determined for T-peel specimens bonded with structural adhesives. Some additional work was undertaken to confirm the locus of the origin of failure.

Photographs were taken during T-peel tests to determine the location and loads where the initial crack forms in the specimen. Experiments were performed using a PU adhesive joint tested at 20 °C and 3 x 10^{-3} s^{-1}. Photographs were taken at 50 N intervals using a digital camera. Subsequent analysis of the photographs indicated that a crack first becomes visible in the photograph taken at a load of 750 N (Figure 5.4a). This is consistent with the levels of load where the T-peel joints had seemed to have 'softened' considerably. The crack forms near the beginning of the curved section of the adherends, far from the end of the fillet, as predicted from the FEA (Figure 25). Subsequent photographs show that the crack grew simultaneously out towards the end of the fillet and back into the joint. The growth appeared to be faster towards the fillet. The crack growth rate was stable but very low (around 2 μm s^{-1}). The maximum load sustained by this joint was 1036 N. Photographs taken at this load (Figure 26) indicate that the crack had not reached the end of the fillet by this load (however, the images were only recorded on one side of the joint and, at the time of testing, observations were not made of the other edge of the joint so it is not known whether crack growth was asymmetrical).

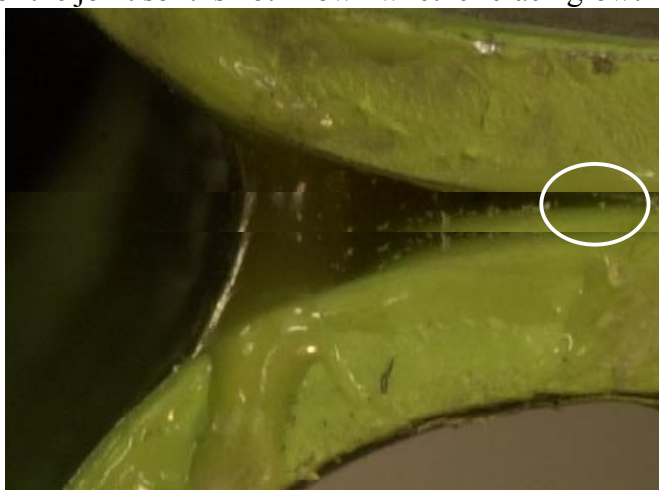

(a) Load 750N – crack becomes visible

(b) 1036 N – maximum load

Figure 26: Crack initiation in the T-peel test (PU adhesive)

6. ADDITIONAL SPECIMEN GEOMETRIES

6.1 BULK ARCAN SPECIMEN TESTS

To test whether the hyperelastic models can accurately predict shear behaviour of the adhesive from tensile input data it was necessary to compare predicted and experimental results from test configurations where shear loading is predominates. In the main, this was done through lap shear tests. However, alternative tests are available. Bulk specimen shear tests remove one of the uncertainties, that there are differences between bulk and bonded adhesive materials, from the analysis of the accuracy of the FE model predictions. The elastomeric adhesive did not have sufficient rigidity to form viable bulk shear test specimens at thickness approaching those of the tensile specimens or adhesive bond lines. However, such specimens could be made from the more rigid PU adhesive.

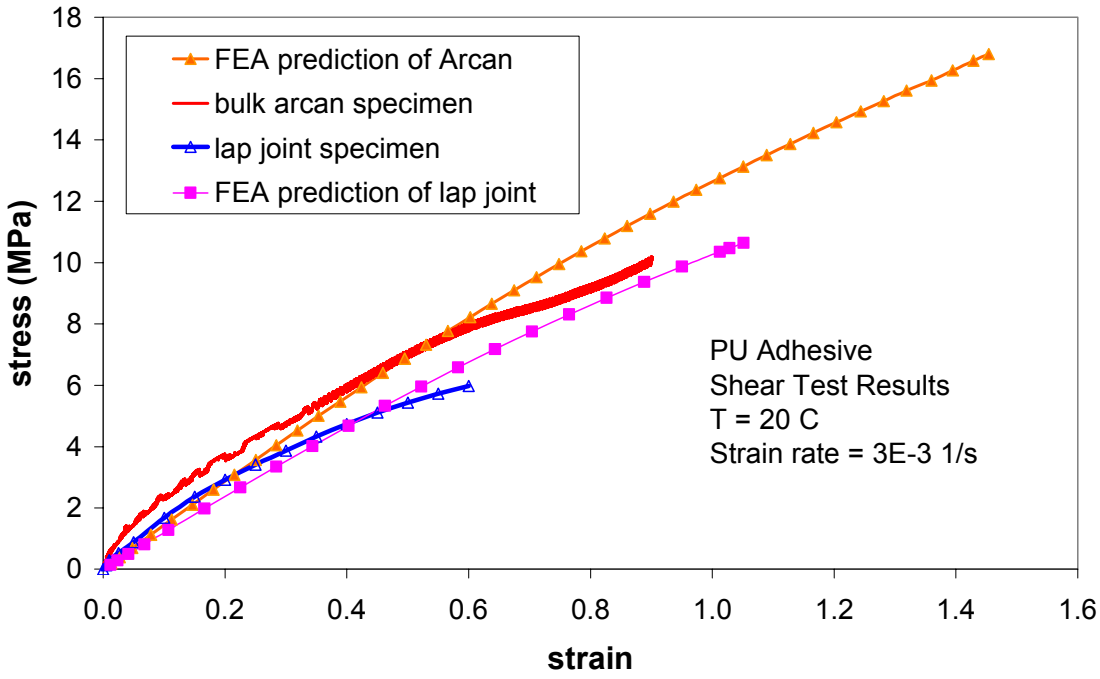

Figure 27: Comparison of measured and predicted shear behaviour for the PU adhesive

The Arcan test is used to determine the properties of bulk specimens of structural adhesives under shear loading [56]. The notched-plate specimen is clamped in a test fixture that imposes a uniform shear stress distribution in the centre of the specimen when it is loaded in a tensile test machine. Shear strains are determined from the relative movement of points either side of the centre line of the specimen. Normally this is done using a special extensometer developed for the specimen [56] but the maximum travel of this device is limited. A video extensometer device that, through image analysis, can track the movement of contrasting dots on the specimen surface was used to overcome this limitation. An FE model of the specimen and fixture was created. A comparison between the measured and predicted deformations is shown in Figure 27, lap shear joint results (modelled using GPE elements) are added for comparison. For both test configurations, the FE predictions are reasonably accurate.

The bulk Arcan specimen fails (around 250 N) through stress concentrations near the notch roots whose location is predicted by the FE stress analysis (locations of these stress concentrations are indicated by arrows in Figure 28). A summary of the maximum values of stress and strain components, predicted at a load of 249 N, is given in Table 27.

Force	E12	EP3	S11	S22	S12	SP3	MISES	SENER
N			MPa	MPa	MPa	MPa	MPa	J/mm^3
248.8	1.14	0.67	12.6	22.8	16.5	33.1	30.0	10.3

Table 27: Stress and strain components at PU Arcan specimen notch roots

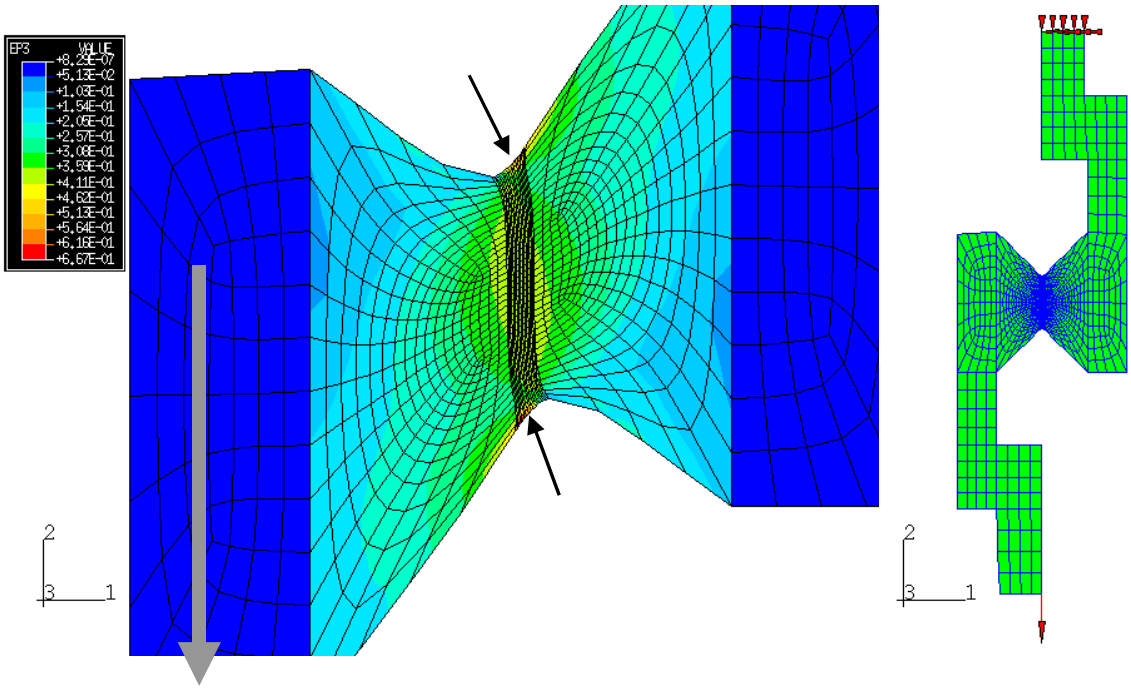

Figure 28: Model of Arcan test specimen

6.2 BUTT TENSION JOINT

The butt tension joint test has been used to evaluate the performance of toughened structural adhesives under triaxial stress fields. Two cylindrical rods are bonded together and pulled in tension. Good alignment during cure and testing is critical for obtaining reliable results. This test is described elsewhere [57]. Some butt joints, bonded with the elastomeric adhesive, were modelled and tested in order to evaluate an additional joint geometry. The results shown in Figure 29 indicate that the butt joint can sustain loads up to around 800 N. The FEA prediction is reasonably accurate until high loads where the specimen softens considerably. This softening may indicate the beginning of specimen rupture although the reasonably long plateau for the final load suggests that crack propagation is slow.

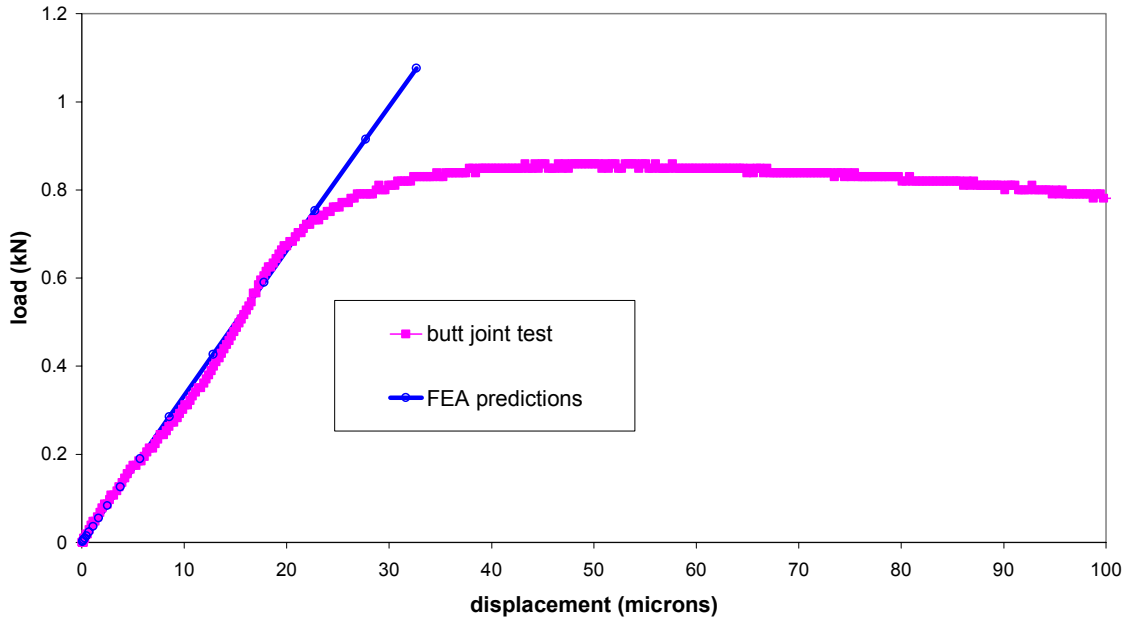

Figure 29: Comparison of measured and predicted butt joint results (elastomeric adhesive)

The predicted maximum stress and strain values in the adhesive layer are shown in Table 28.

Specimen	Load	E12	EP3	S11	S22	S12	SP3	MISES	SENER
	N			MPa	MPa	MPa	MPa	MPa	J/mm^3
Butt	859	0.13	0.09	2.98	2.57	0.55	2.98	1.24	0.07

Table 28: Predicted stress and strain components in the butt tension test

6.3 PLANAR TENSION TEST

The planar tension test [38, 39] was one of the test methods originally developed in order to obtain the full suite of input data sets for the hyperelastic models. Short, wide specimens are pulled in tension with grips that constrain lateral contractions. The resulting strain field is assumed to be plane strain. An FE model was created of the planar test specimen and run using uniaxial tension data as the input. The predicted force-extension behaviour closely matches the experimental measurements (Figure 30). The planar test specimen starts to fail at the corners and the FEA predicts stress concentrations in these areas (Figure 31). A summary of the predicted stress and strain components is shown in Table 29.

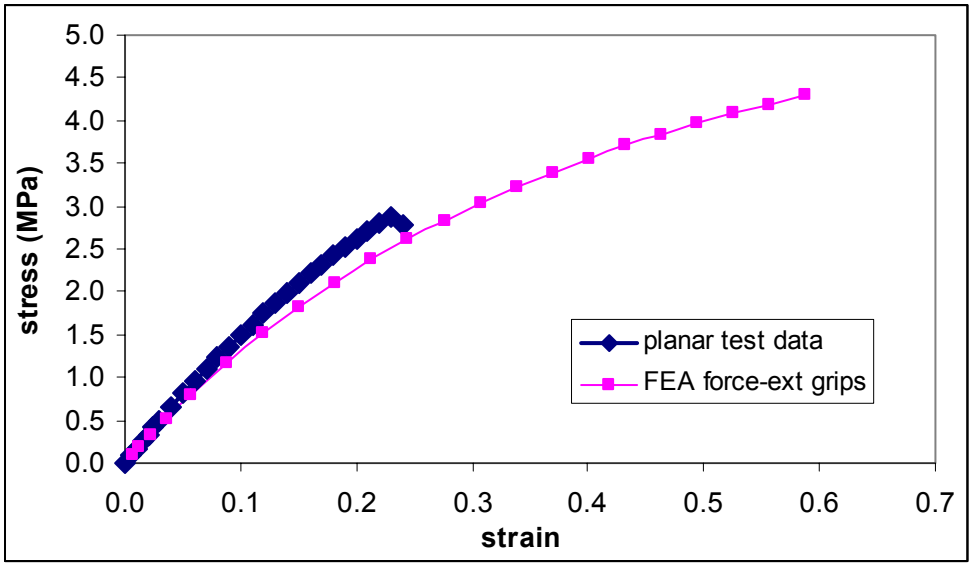

Figure 30: Comparison of measured and predicted planar tension data (elastomeric adhesive)

Load	E12	EP3	S11	S22	S12	SP2	MISES	SENER
N			MPa	MPa	MPa	MPa	MPa	J/mm^3
523	0.394	3.41	2.22	3.5	1.42	4.41	3.93	0.677

Table 29: Predicted stress and strain components in the planar specimen

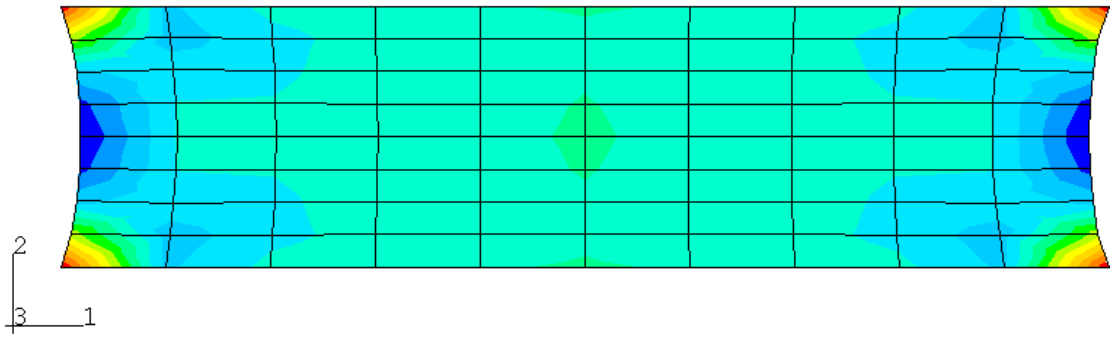

Figure 31: Stress distribution in planar tension specimen

7. ADHESIVE JOINT FAILURE

7.1 ELASTOMERIC ADHESIVE

The failure mode of elastomeric adhesive joints was invariably cohesive in the adhesive layer. Thick layers of adhesive remain on both adherends after the joints are pulled apart. This adhesive is a black colour and it is extremely difficult to visually detect any cracks within the glue line. Since it is a soft, lossy material, rupture of the material emits very little acoustic energy and there is no characteristic crack heard during the test. However, some observations suggest that, in lap joint specimens with fillets, failure initiates in the fillets near the corner of the adherend. This is the region where FEA predicts the stress concentration.

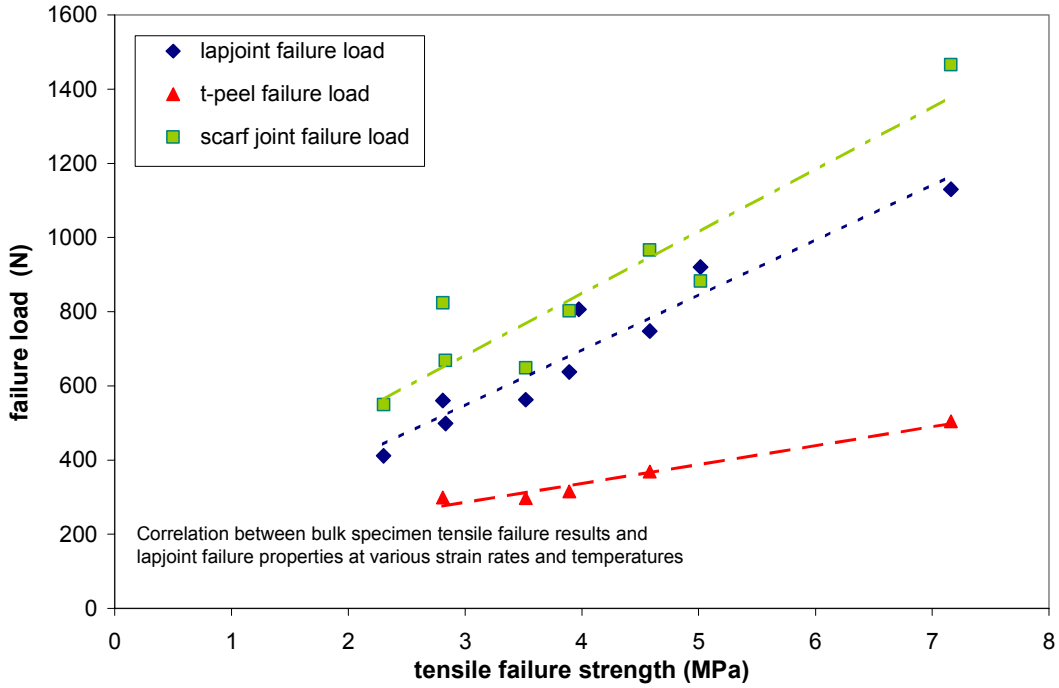

Figure 32: Correlation between failure loads and tensile strength for elastomer adhesive

The failure loads of joints bonded with this adhesive should correlate with the material strength of the bulk adhesive samples since the mode of failure is through cohesive rupture of the adhesive. The failure loads of both the bulk material and joint specimens depend on temperature and strain rate. Plots of average maximum joint load against tensile failure strength at corresponding temperatures and strain rates are shown in Figure 32. For each type of joint specimen (lap joint, scarf joint and T-peel) there is a reasonable linear relation between the two. This suggests that there may be a single failure criterion, related to the tensile strength, which could predict failure in the joints. FEA of lap joint specimens suggests that there is a linear relationship between the maximum values of stress components, such as peel stress (S22) or maximum principal stress (SP3), at maximum load and the tensile failure strength.

The stress components predicted in the lap joint happen at a corner in the specimen where the solution predicts a singularity. Therefore, the maximum values predicted are strongly dependent on the size of element at this corner. The stress and strain components predicted by FEA are true stress and true strain components and should be compared with the true stress and true strain results from the uniaxial tension test and not the apparent values.

Geometry	Load	E12	EP3	S11	S22	S12	SP3	MISES	PRESS	SENER
	N			MPa	MPa	MPa	MPa	MPa	MPa	J/mm^3
Lap joint – 1 mm fillet (Figure 11c)	612	0.50	0.27	3.24	1.83	2.15	3.95	3.84	-2.24	0.57
Lap joint – no fillet (Figure 11a)	612	0.63	0.34	2.81	2.88	2.68	5.53	4.67	-3.05	0.88
Lap joint – curved fillet (Figure 11d)	612	0.45	0.26	3.83	2.15	1.97	4.37	3.65	-3.01	0.57
Lap joint – small fillet (Figure 11b)	612	0.55	0.30	2.80	1.57	2.43	4.46	4.43	-2.30	0.74
Scarf joint 30°	802	0.14	0.19	2.86	0.47	0.55	3.06	2.64	-1.73	0.31
Scarf joint 45°	571	0.00	0.12	2.26	0.56	0.02	2.26	1.63	-1.12	0.14
Butt joint	859	0.13	0.09	2.98	2.57	0.55	2.98	1.24	-2.71	0.07
T-peel	350	0.17	0.12	4.57	3.89	0.73	4.57	1.52	-4.10	0.17
Bulk uniaxial tensile	14.8	0	0.38	4.2	0	0	4.2	4.2	-1.40	0.82
Bulk planar tension	523	0.45	0.33	3.59	2.08	1.83	3.96	3.79	-1.98	0.68

Table 30: Comparing FEA predicted stress and strain component values in different elastomeric adhesive specimen geometries tested at 20 °C and $3x10^{-3}s^{-1}$

Various stress and strain components are compared for different adhesive joint and bulk specimen geometries in Table 30. There is a large spread between the values. The SP3 (maximum principal stress) values for the lap joint, T-peel and bulk test specimens appear to correlate reasonably well. However, SP3 values are lower in the scarf and butt tension tests (the butt tension test might be considered a 90° scarf test). FEA predictions suggest that any type of fillet can relieve stress concentrations in the lap joint test. Von Mises stress values are comparable in the lap joint and bulk specimens but are considerably lower in the T-peel, scarf and butt joint specimens. In the T-peel and butt joint tests the hydrostatic pressure (PRESS) components are more significant. There might be some scope for considering a modified von Mises criterion, combining von Mises and hydrostatic pressure stress states, as a failure criteron if the scarf results are ignored. Strain energy density (SENER) values are too variable for use as a universal failure criterion. The Tresca stress values are similar to the von Mises predictions (although around 10 % higher).

While arguments can be made for correlating the maximum principal stress values found in bulk specimen tests with those predicted at failure in the lap joint and T-peel tests, the butt joint tests and, particularly, the scarf joint tests do not fit this correlation. Figure 33 shows plots of predicted SP3 values against corresponding tensile strengths for lap joint (no fillet), lap joint (with small fillet), scarf and T-peel joints. The same trends, as those indicated in Table 30, can be seen. Straight lines can be fitted to the curves and the results are summarised in Table 31. The differing slopes suggest that the correlations described above may not hold for different test conditions.

Joint Type	Slope	Intercept	r^2
Lap joint – no fillet	1.604	1.7	0.90
Lap joint - fillet	1.038	1.07	0.91
Scarf (30°)	0.724	1.69	0.98
T-peel	0.494	0.98	0.91

Table 31: Regression of maximum principal stress-tensile strength curves (elastomeric)

It is generally observed that the presence of fillets reduces the stress concentration in the adhesive bond layer. In the analyses of the 'no fillet' and 'long fillet' cases the maximum stress was reduced by around 25 % when the fillet was added to the model (the stress concentration also moved from the interface with the continuous adherend to the corner of the adherend). However, the experimental gain in strength was not particularly significant. It is not known if this indicates some artefact of the model where the numerical singularities at the different critical areas lead to different predicted stress concentration factors or whether the low gain in strength is due to experimental factors, such as cure history.

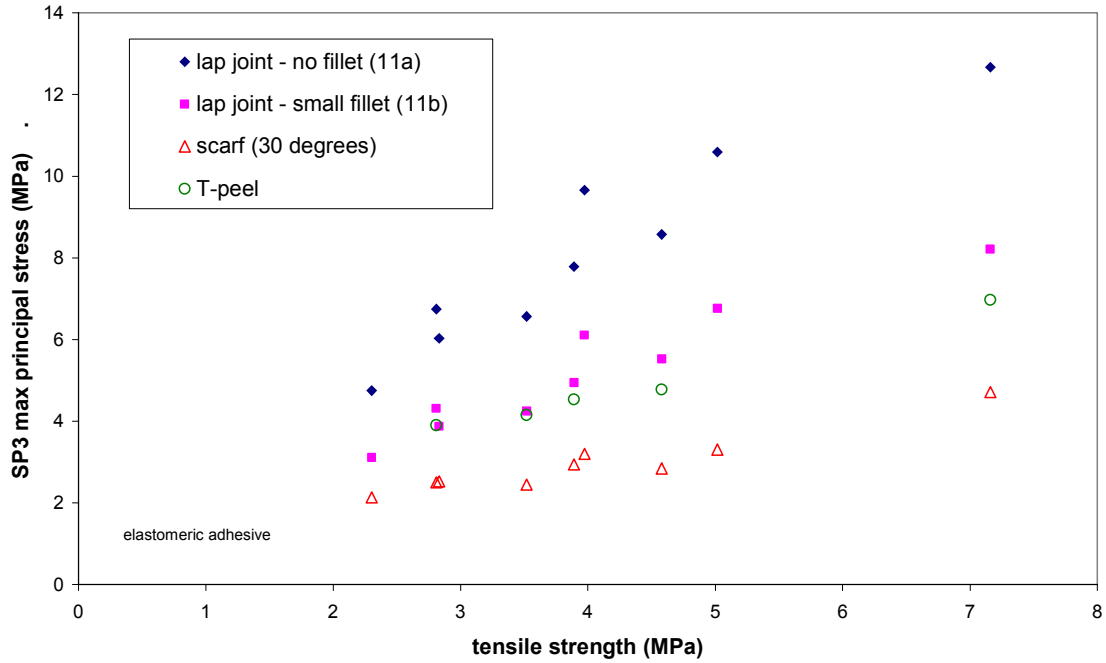

Figure 33: Correlation of predicted SP3 and tensile strength values at different strain rates and temperatures for elastomeric adhesive joints

The durability of the flexible adhesive has not been considered in this work. However, some uniaxial test specimens were exposed to water and tested after several months when they had absorbed approximately 4 % moisture by weight [58]. The tensile results on the exposed specimens showed a considerable increase in stiffness at low strains (some 50% or higher increase in modulus) but very much reduced strain and, thus, stress at failure. The increase in modulus is surprising as the normal assumption is that adsorbed moisture leads to plasticisation of the material and a reduction in stiffness. There may be fundamental differences between the effects of moisture on flexible adhesives and the effects of moisture on rigid, structural adhesives such as epoxies.

7.2 POLYURETHANE ADHESIVE

In contrast to the elastomeric adhesive, the failure modes for joints bonded using the polyurethane are a mixture of adhesive failure, primer failure and cohesive failure in the adhesive. Therefore, it seems unlikely that there can be a single criterion that will predict failure in all circumstances. As with the elastomeric adhesive the failure loads of both the bulk test and joint test specimens vary with strain rate and temperature and this needs to be considered in any design procedure. This is illustrated in Figure 34, where the lap joint, maximum scarf and T-peel failure loads correlate with tensile strength. The averaged scarf joint results are more scattered.

Photographic evidence shows that cracks form in the polyurethane adhesive joints prior to ultimate load. In many cases, the cracks become visible at 50 % or less of the ultimate load reached. In each case the site of crack initiation corresponded to the location of stress concentrations predicted by the FEA.

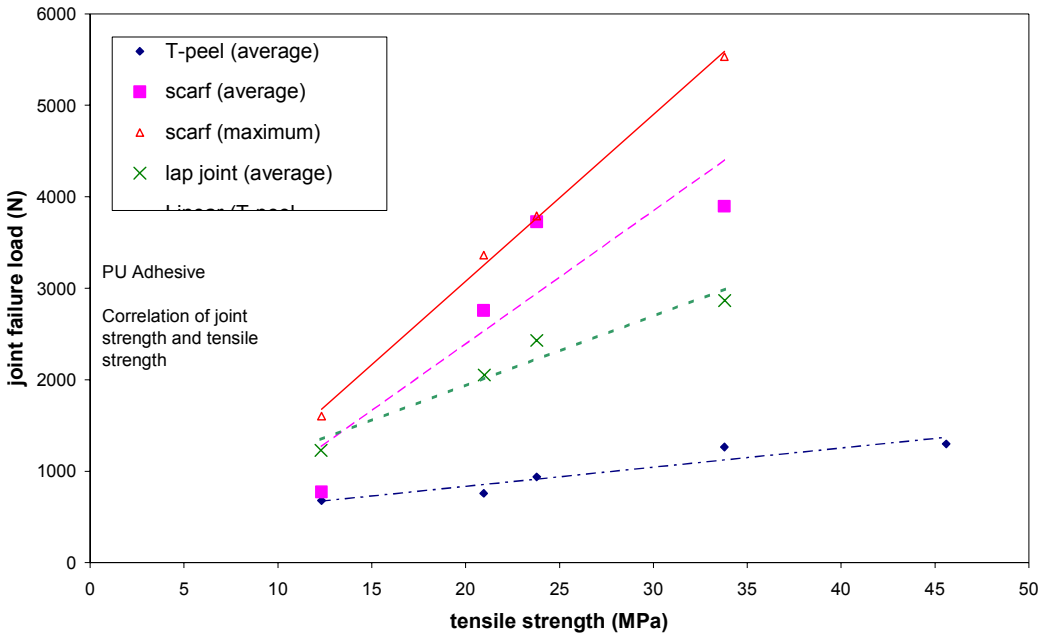

Figure 34: Correlation between failure loads and tensile strength for PU adhesive

Table 31 compares predicted stress and strain components in different PU bulk and joint test specimens. The maximum principal stress values are reasonably consistent between the joint types but are well down on the bulk specimen values. The SP3 values range from 15 to 20 MPa and are close to the average engineering stress at failure in the tensile tests (16 MPa). However, they are considerably lower than the true stress values at failure in the tensile test (over 30 MPa). Unlike the elastomeric adhesive, the SP3 predictions for the scarf joints are not noticeably lower than for the other joints but it should be noted that the scarf loads used were the highest measured and not the average failure loads presented for the other joints. The von Mises and the hydrostatic pressure predictions follow the same trends as in the elastomeric adhesive. Once again, the strain energies vary widely and do not provide a basis for a failure criterion.

Specimen	Force	E12	EP3	S11	S22	S12	SP3	MISES	PRESS	SENER
	N			MPa	MPa	MPa	MPa	MPa		J/mm^3
Tensile	88	0	0.77	30.9	0	0	30.9	30.9	-10.3	11.1
Lap (no fillet)	2325	0.73	0.42	11.25	10.40	9.96	20.81	17.43	-10.36	4.30
Lap (long fillet)	2325	0.55	0.31	11.6	6.51	7.66	14.49	13.75	-7.80	2.56
T-peel	937	0.12	0.54	0.177	12.24	1.69	20.02	5.36	-13.01	1.48
Scarf	3790	0.31	1.77	0.33	15.85	2.47	15.70	13.50	-8.39	2.56
Arcan	249	1.14	0.67	12.6	22.8	16.5	33.1	30.0	-16.3	10.3

Table 31: Comparing FEA predicted stress and strain component values in different PU specimen geometries tested at 20 °C and $3x10^{-3}s^{-1}$

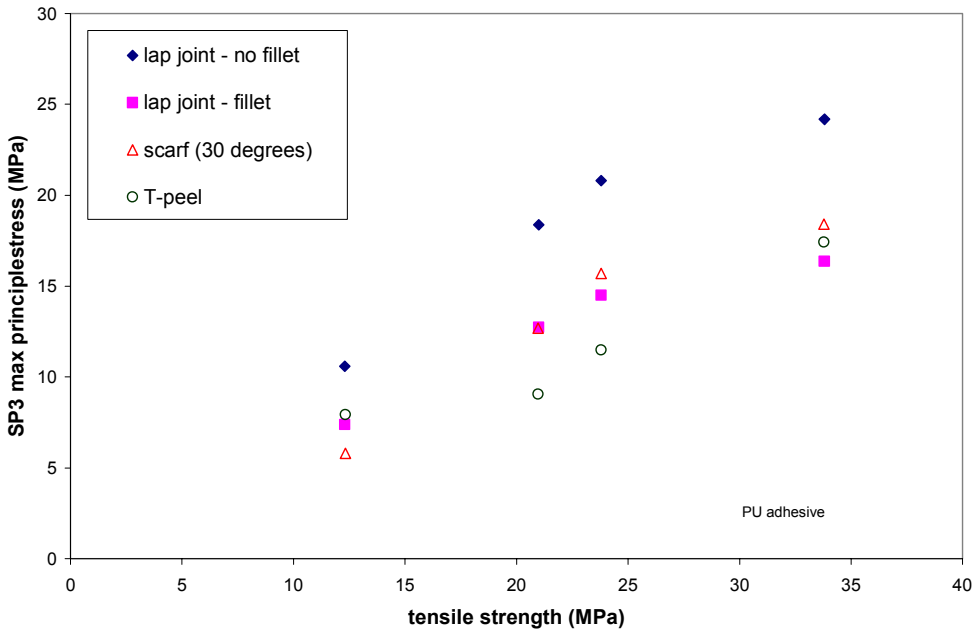

Figure 35: Correlation of predicted SP3 and tensile strength values at different strain rates and temperatures for PU adhesive joints

8. CONCLUDING REMARKS

The provision of an accurate failure criterion for adhesives would greatly facilitate accurate modelling of adhesively bonded structures. Much work has been performed on structural adhesives and still no universal criterion has been established. Flexible adhesives have received much less attention than structural adhesives and, so, this work has had to concentrate more on the mechanics of characterising and modelling the material properties than on failure mechanisms. The focus of the work reported here has been to compare different types of adhesive joint in order to establish commonality between stress and strain states in the regions of the specimen critical to failure.

The results show that the load bearing capacity of the various types of joint correlate well with the tensile strength of the adhesives at the corresponding strain rate and temperature. This suggests that the joint strength is a function of the material strength. The different joints all have significantly different stress fields and the most obvious way to compare them is through FEA. Unfortunately, there does not appear to be any simple universal stress, strain or strain energy component that reaches consistent values for different joints at failure.

Part of this failure to identify a simple criterion at failure may be traced back to inadequacies of the models to accurately predict the force-extension behaviour of the various types of joints. The FEA predictions are all much more linear than the actual measured joint behaviour. The linearity of the FEA predictions can be traced back to the linearity of the measured uniaxial tension stress-strain curves that feeds through into the model predictions. The resulting predictions have a tendency to be stiffer than the measurements and, therefore, predictions at the failure load of the joint will tend to underestimate the strains in the joint.

A further likely reason for the inability of any single criterion to describe failure is the difficulty that FEA has in handling sharp corners or material discontinuities in the models. These lead to numerical singularities in the solution and predicted stress concentrations, which depend significantly on the element density near the critical region. Differing sensitivities of the stress concentration to the element size for different joint geometries mean that, even when element sizes are similar in models, it is difficult to confidently compare the predicted stress/strain values. Greater confidence can be placed on stress predictions where the region of maximum stress or strain covers several elements, as the dependence of the results on the mesh density should be minimal. Of the joints investigated, only the T-peel joint gave stress concentrations covering several elements. With certain precise fillet shapes and assumed curvatures of the adherend corners, stress distribution predictions can be achieved in lap joints where the stress concentration covers several elements (although due to the detail required to represent the geometry the element size is necessarily small). Such detailed modelling (and specimen preparation) is time consuming and costly to perform.

Where observations of the formation of cracks in the PU specimens were made, they were detected significantly before the ultimate load reached in the test. Although the analyses were made for the ultimate load in the specimens, it is likely that the point in the test where the failure criterion should apply is the point at which cracks appear. This could be as much as 50% below the ultimate load. The stress predictions at maximum load are significantly lower than the strength of the bulk material. At the point of failure initiation the stress levels will be lower still – perhaps 25% to 30% of the bulk material strength. It is debatable whether the initiation of cracks can be correlated to conditions pertaining to the rupture of the bulk material given the presence of additional multi-axial and hydrostatic stress in a joint. The elastomeric adhesive is black and it is difficult to detect the presence of cracks in any of the specimens. All

attempts to detect cracks prior to failure have yielded ambiguous results. It is possible that the point of maximum force in these tests corresponds with the appearance and growth of a fracture.

In comparison to the bulk specimen strengths and the other joint types, the scarf specimens appear weaker than expected. The predicted maximum stress values in these specimens are lower than in other configurations. Results of these tests may have been compromised by suspected differences in cure state for the 1-part adhesive or mixing/dispensing difficulties for the 2-part adhesive.

Given the uncertainty in the interpretation of the FEA stress concentrations and the potential inaccuracy of the material models used to characterise the flexible adhesives, it is unrealistic to define a definitive failure criterion. Indeed, in the light of material variability and potential degradation on ageing, this could be positively misleading. The maximum principal stress is probably as suitable as any of the criteria investigated. This seems to scale with material strength in different joint types. The maximum allowable maximum principal stress in the joint should not exceed a defined fraction of the tensile strength of the material. This fraction will depend on the material. The results determined in this work suggest that the elastomeric adhesive joint can sustain a higher proportion of its tensile strength than the PU adhesive.

Whilst a failure criterion has not been established, this work has generated a better understanding of the performance of flexible adhesives. The following observations should be noted.

- Flexible adhesives can be modelled using hyperelastic material models, however the predictions of the behaviour of the bonded joints can be inaccurate due to a number of reasons. In general:
    - First-order material models such as Arruda-Boyce, Mooney-Rivlin or Neo Hooke seem most appropriate for flexible adhesives.
    - Predictions are more linear than measurement. However, true stress-strain plots of tensile data are essentially linear.
    - Input data for hyperelastic models can be obtained from uniaxial test data. There does not appear to be any significant gain in accuracy from the addition of planar or biaxial test data.
    - Flexible adhesives are compressible and volumetric terms need to be included in the material models. Data for these can be determined from contraction measurements in uniaxial tension tests.
    - The predicted stress distributions and concentrations in the adhesive bond layer do not appear to have any significant dependence on material model, general element type or input data types – factors that do affect the predicted force-extension behaviour.
    - The predicted stress distributions and concentrations in the adhesive bond layer depend on joint end geometries and element sizes – factors that have only a limited influence on the predicted force-extension behaviour.
    - 2-dimensional plane strain element predictions tend to be in good agreement with 3-dimensional model predictions. However, generalised plane strain element predictions tend to show higher curvatures and, thus, match better the experimental measurements.
- The properties of the flexible adhesives depend on temperature and strain rate:
    - Models should be supplied with input data corresponding to the rates and temperatures under which they are modelled.

    - Failure strength is strain rate and temperature dependent.
    - There are correlations between the loads under which joints fail and the tensile strength of the adhesives under corresponding conditions.
    - A conservative estimation of strength can be made through testing the adhesive or joint at an elevated temperature and slow test speed. It may be possible to use a time-temperature superposition approach to predict strengths. The elevated temperature/slow strain rate testing approach could also be used for the estimation of creep strengths.
- The strength of flexible adhesive joints depends on joint geometry.
    - Failure loads, normalised by bonded area, appear reasonably constant for scarf and lap shear joints.
    - The strengths of scarf joints fall as the taper angle is increased. The location of the stress concentration varies for different angles.
- The shape and size of the fillet influences joint strength
    - The addition of a fillet reduces the stress concentration at the end of the lap joint specimen and improves load-bearing capacity.
    - If a fillet exceeds a certain length or height then there is no significant load in the exterior of the fillet and the stress concentration is independent of the exact geometry of the fillet. Leaving adhesive flash on lap joints could improve reproducibility of lap shear tests.
    - The stress concentration predicted in the T-peel specimen is in the interior of the fillet and, therefore, it could be expected that the exact shape of the fillet does not have significant influence on the strength. This is in contrast to findings for rigid, structural adhesives.
- Rupture of the adhesive has been observed to occur significantly below the ultimate strength of the joints. Design criteria should be selected to avoid this happening.

Although no obvious failure criteria have been identified, it would seem prudent to ensure that the maximum principal stress in the adhesive layer does not exceed some fraction of the tensile strength of the bulk adhesive. Some adhesives appear to tolerate stress levels at a higher proportion of their tensile strength than others. The scaling factor for strength would have to be decided on an adhesive-by-adhesive basis.

Acknowledgements

This work was sponsored by the Department of Trade and Industry and carried out as part of project PAJex2, Flexible Adhesives, of the Performance of Adhesive Joints programme. The authors would like to thank the members of the PAJ Industrial Advisory Group for their support and encouragement. 3M Ltd and Evode Ltd are acknowledged for supplying materials.

The authors are grateful to Greg Dean, George Hinopolous, Keith Ogilvy-Robb, Tony Maxwell and Roger Hughes at NPL for assistance with the research.

References

1. L R G Treloar, Trans. Faraday Soc., 40, 1944
2. E M Arruda and M C Boyce, J. Mech. Phys. Solids, vol. 41(2), 1993
3. R W Ogden, Proc. R. Soc. Lond. A. 326, 1972
4. L R G Treloar, The Physics of Rubber Elasticity, Second Edition, Oxford University Press, 1958
5. A R Johnson, C J Quigley and J L Mead, Rubber Chemistry and Technology, vol 67, 1994.
6. A R Johnson, J L Mead and C J Quigley, Rubber Chemistry and Technology, vol 68, 1995.

7. Hart-Smith, L.J., "Adhesive-Bonded Single-Lap Joints", NASA Report CR-112236, 1973.
8. Hart-Smith, L.J., "Adhesive-Bonded Scarf and Stepped-Lap Joints", NASA Report CR-112237, 1973.
9. Hart-Smith, L.J., "Adhesive-Bonded Double-Lap Joints", NASA Report CR-112238, 1973.
10. Hart-Smith, L.J., "Analysis and Design of Advanced Composite Bonded Joints", NASA Report CR-2218, 1974.
11. Harris, J.A. and Adams, R.D., "Strength Prediction of Bonded single Lap Joints by Non-Linear Finite Element Methods", International Journal of Adhesion and Adhesives, Volume 4, Number 2, 1984, pp 65-78.
12. Adams, R.D., "The Mechanics of Bonded Joints, Structural Adhesives in Engineering, ImechE Conference Publications, Suffolk, 1986, pp 17-24.
13. "Adhesives and Sealants", Engineered Materials Handbook, Volume 3, ASM International, 1990.
14. Composites Engineering Handbook", Edited by Mallick, P.K., Marcel Dekker, Inc., 1997.
15. Olusanya A, A criterion of tensile failure for Hyperelastic materials and its application to viscoelastic-viscoplastic materials, NPL Report CMMT(B)130, April 1997.
16. "Mechanical Properties of Solid Polymers", Ward, I.M., John Wiley & Sons, Ltd, 1971.
17. "Introduction to Polymers", Young, R.J., Chapman and Hall, 1981.
18. Bowden, P.B. and Dukes, J.A., "The Plastic Flow of Isotropic Polymers", Journal of Materials Science, Volume 7, 1972, pp 52-63.
19. Wang, C.H. and Chalkley., "Plastic Yielding of A Film Adhesive Under Multiaxial Stresses", International Journal of Adhesion and Adhesives, Volume 20, Number 2, 2000, pp 155-164.
20. Dean, G.D. and Crocker, L., "Comparison of the Measured and Predicted Deformation of an Adhesively Bonded Lap-Joint Specimen", NPL Report CMMT(A)293, 2000.
21. Read, B.E., Dean, G.D. and Ferriss, D.H., "An Elastic-Plastic Model for the Non-Linear Mechanical Behaviour of Rubber-Toughened Adhesives", NPL Report CMMT(A)289, 2000.
22. Gurson, A.L., "Continuum Theory of Ductile Rupture by Void Nucleation and Growth: Part 1 – Yield Criteria and Flow Rules for Porous Ductile Meadia", Journal of Engineering Materials Technology, Transactions of ASME, Volume 99, 1977, pp 2-15.
23. Lazzeri, A. and Bucknall, C.B., "Dilatational Bands in Rubber-Toughened Polymers", Journal of Materials Science, Volume 28, 1993, pp 6799-6808.
24. "Physics of Glassy Polymers", Second Edition, Edited by Haward, R.N. and Young, R.J., Chapman and Hall, London, 1997.
25. Groth, H.L., "A Method to Predict Fracture in an Adhesively Bonded Joint", International Journal of Adhesion and Adhesives, Volume 5, Number 1, 1985, pp 19-22.
26. Groth, H.L., "Stress Singularities and Fracture at Interface Corners in Bonded", International Journal of Adhesion and Adhesives, Volume 8, Number 2, 1999, pp 107-113.
27. Fernlund, G. and Spelt, J.K., "Failure Load Prediction: I. Analytical Method", International Journal of Adhesion and Adhesives, Volume 11, Number 4, 1991, pp 213-220.
28. Fernlund, G. and Spelt, J.K., "Failure Load Prediction: II. Experimental Results", International Journal of Adhesion and Adhesives, Volume 11, Number 4, 1991, pp 221-227.
29. Fernlund, G., Papini, M., McCammond, D. and Spelt, J.K., "Fracture Load Predictions for Adhesive Joints", Composites Science and Technology, Volume 51, 1994, pp 587-600.
30. Ashcroft, I.A, Gilmore, R.B and Shaw, S.J., "Cyclic Fatigue and Environmental Effects with Adhesively Bonded Joints", AGARD 83rd SMP Meeting, Florence, 1996.
31. Curley, A.J., Hadavinia, H., Kinloch, A.J. and Taylor, A.C., "Predicting the Service-Life of Adhesively-Bonded Joints", International Journal of Fracture, Volume 103, 2000, pp 41-69.
32. Towse, A., Potter, K.D., Wisnom, M.R. and Adams, R.D., "The Sensitivity of a Weibull Failure Criterion to Singularity Strength and Local Geometry Variations", International Journal of Adhesion and Adhesives, 19, 1999, pp 71-82.
33. Duncan B, Hinopoulos H, Ogilvy-Robb K and Arranz E, Rate and temperature dependent properties of a flexible adhesive, CMMT(A)262, 2000.
34. Duncan B, Hyperelastic properties of a polyurethane adhesive, MATC(A)23, 2001
35. Crocker L and Duncan B, Measurement methods for obtaining volumetric coefficients for hyperelastic modeling of flexible adhesives, CMMT(A)286, 2001
36. Duncan B, Preparation of bulk adhesive test specimens, CMMT(MN)057, 1999

37. Dean G and Duncan B, Preparation and testing of bulk specimens of adhesives, NPL Good Practice Guide No 17, 1998.
38. Duncan B C, Maxwell A S, Crocker L E and Hunt R A**,** Verification of Hyperelastic test methods, CMMT(A)226, October 1999.
39. Duncan B, Test methods for determining hyperelastic properties of flexible adhesives, CMMT(MN)054, 1999
40. Duncan B, Crocker L and Urquhart J, Evaluation of hyperelastic finite element models for flexible adhesive joints, CMMT(A)285, 2000.
41. "ABAQUS User's Manual", Version 5.8, HKS Inc., USA, 1998.
42. "FEMGV User's Manual", Version 5.1, FEMSYS Ltd., 1998.
43. Crocker L E, Duncan B C, Hughes R G and Urquhart J M, Hyperelastic modeling of flexible adhesives**,** CMMT(A)183, May 1999.
44. Broughton, W.R. and Hinopoulos, G., "Evaluation of the Single-Lap Joint Using Finite Element Analysis", NPL Report CMMT(A)206, 1999.
45. BS EN 1465:1995, "Adhesives - Determination of Tensile Lap-shear Strength of Rigid-to-Rigid Bonded Assemblies".
46. BS EN ISO 9664:1995, "Adhesives - Test Methods for Fatigue Properties of Structural Adhesives in Tensile Shear".
47. C C Chamis and P L N Murthy, Simplified Procedures for Designing Adhesively Bonded Composite Joints, J. of Reinforced Plastics and Composites, Vol 10, pp29-41, 1991.
48. Broughton W, Size Effects on the Performance of Flexible Adhesive Joints, Measurement Note MATC(MN)11, 2001
49. Broughton W R, Hinopoulos G and Mera R D, Cyclic fatigue testing of adhesive joints, test method assessment**,** CMMT(A)191, 1999.
50. ASTM D 1876. Standard test method for peel resistance of adhesives (T-peel test), Volume 15.06, ASTM Standards, 1995, 105-107.
51. ISO 11339: 1993. Adhesives - 180° Peel test for flexible-to-flexible bonded assemblies (T-peel test).
52. Experimental assessment of durability of test methods. MTS Adhesive Programme, Project 3: Environmental durability of adhesive bonds, Report No 8, AEA Technology, Harwell, United Kingdom, 1995.
53. Broughton, W R and Mera, R D Review of durability test methods and standards for assessing long term performance of adhesive joints, NPL Report CMMT(A)61, 1997.
54. Hinopoulos G and Broughton W, Evaluation of the T-peel joint using the Finite Element method, NPL Report CMMT(A)207, 1999.
55. Broughton W R, Mera R D and Hinopoulos G. Static fatigue testing of adhesive joints - T-peel test. *PAJ Project 3 - Report 13*, NPL Report CMMT(A) 193, 1999.
56. B C Duncan and G D Dean; Test Methods for Determining Shear Property Data for Adhesives Suitable for Design - Part 1: Notched-Beam (Iosipescu) and Notched-Plate (Arcan) Methods for Bulk and Joint Test Specimens, NPL Report CMMT(B)56, April 1996.
57. Crocker L and Dean G, Tensile Testing of Adhesive Butt Joint Specimens, NPL Measurement Note MATC(MN)09, 2001
58. Duncan B, Effects of moisture on the mechanical properties of M70 Adhesive, NPL Report MATC(B)29, 2001.

APPENDIX I

GLOSSARY OF ABAQUS STRESS AND STRAIN COMPONENTS

Type	Name	Definition
Stress Component	S11 S22 S33 S12	Stress in 1 direction (tensile stress) Stress in 2 direction (peel stress) Stress in 3 direction (through width) Shear Stress (Directions as defined by axes in model, stress values are true stress)
Strain Components	E11 E22 E33 E12	Strain in 1 direction (tensile strain) Strain in 2 direction (peel strain) Strain in 3 direction (through width – normally negligible) Shear Strain (Directions as defined by axes in model, strains are true strains)
Principal Stress Components	SP1 SP2 SP3	Minimum principal stress (σ_1) Intermediate principal stress (σ_2) Maximum principal stress (σ_3) (Orthogonal axes aligned with direction of maximum stress, stress values are true stress)
Principal Strain Components	EP1 EP2 EP3	Minimum principal strain Intermediate principal strain Maximum principal strain (Orthogonal axes aligned with direction of maximum stress, strains are true strains)
Stress Invariants	MISES TRESC PRESS INV3	Mises equivalent Stress (τ_m) $6\tau_m^2 = (\sigma_1 - \sigma_2)^2 + (\sigma_2 - \sigma_3)^2 + (\sigma_3 - \sigma_1)^2$ Tresca equivalent shear stress (determined from the maximum difference between principal stresses) $\tau_{max} = \frac{1}{2}(\sigma_1 - \sigma_3)$ Equivalent hydrostatic pressure stress $p = -\frac{\sigma_1 + \sigma_2 + \sigma_3}{3}$ Third stress invariant $\left(r = \left[\frac{9}{2} \right] S_{ij} S_{jk} S_{ki} \right)^{1/3}$
Strain Energy	SENER	Elastic strain energy per unit volume